International Journal of Pharmaceutics 668 (2025) 124952

Contents lists available at ScienceDirect

International Journal of Pharmaceutics

journal homepage: www.elsevier.com/locate/ijpharm

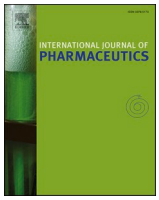

Combination of gold nanoparticles with near-infrared light as an alternative approach for melanoma management

Joana Lopes [a], Carla M. Rodrigues [b], Ana Godinho-Santos [a], João M.P. Coelho [c], Luís C. Cabaço [d], Duarte C. Barral [d], Pedro Faísca [e], José Catarino [f,g], Daniela Nunes [h], Elvira Fortunato [h], Rodrigo Martins [h], Cecília M.P. Rodrigues [a], Maria Manuela Gaspar [a,c,*], Catarina Pinto Reis [a,c,*]

[a] Research Institute for Medicines (iMed.ULisboa), Faculty of Pharmacy, Universidade de Lisboa, Av. Professor Gama Pinto, Lisboa 1649-003, Portugal
[b] REQUIMTE - LAQV, Chemistry Department, NOVA School of Science and Technology, NOVA University Lisbon, Campus da Caparica Caparica 2829-516, Portugal
[c] Instituto de Biofísica e Engenharia Biomédica (IBEB), Faculdade de Ciências, Universidade de Lisboa, Campo Grande 1749-016, Lisboa, Portugal
[d] iNOVA4Health, NOVA Medical School, Faculdade de Ciências Médicas, NMS, FCM, Universidade NOVA de Lisboa, Campo dos Mártires da Pátria, 130, Lisboa 1169-056, Portugal
[e] CECAV- Centro de Ciência Animal e Veterinária- Faculdade de Medicina, Veterinária de Lisboa- Universidade Lusófona-Centro Universitário de Lisboa, Portugal
[f] Faculty of Veterinary Medicine, Universidade Lusófona-Centro Universitário de Lisboa, Portugal
[g] School of Animal Health, Protection and Welfare, Lusophone Polytechnic Institute, Lisbon, Portugal
[h] Department of Materials Science, NOVA School of Science and Technology, Campus de Caparica, i3N/CENIMAT, Caparica 2829-516, Portugal

A R T I C L E I N F O

Keywords:
Nanomedicine
Photothermal therapy
Gold nanoparticles
Melanoma
In vitro models
In vivo models

A B S T R A C T

Melanoma is the most aggressive type of skin cancer and recently approved drugs are often associated with resistance and significant adverse effects. Therefore, the design of more effective and safe options remains imperative. Photothermal therapy (PTT) using gold nanoparticles (AuNPs) presents a promising and innovative approach. In this work, the efficacy of combining a previously optimized formulation of AuNPs coated with a mixture of hyaluronic and oleic acids (HAOA-AuNPs) with near-infrared (NIR) laser irradiation in melanoma cell lines was explored. Coated and uncoated AuNPs formulations were characterized in physicochemical, morphological and elemental terms. Next, the cellular uptake efficiency as well as antiproliferative activity of the combination of each formulation with laser irradiation was evaluated. Subsequently, HAOA-AuNPs were selected to assess the underlying mechanism of combined therapy by cell cycle and Annexin V/PI assays. An *in vivo* syngeneic murine melanoma model was also conducted. *In vitro* studies demonstrated that 24 h after incubation and in the absence of laser, HAOA-AuNPs did not exhibit cytotoxic effects on the melanoma cell lines tested, similar to the laser alone. On the contrary, the combination therapy resulted in a large reduction in cell viability. Furthermore, it has been shown to promote S-phase cell cycle arrest and increase in the percentage of late apoptotic cells. Finally, the *in vivo* proof-of-concept showed that the intratumoral administration of HAOA-AuNPs followed by three laser irradiations impaired tumor progression. Collectively, AuNP-based PTT holds significant potential to improve treatment efficacy and safety, offering a versatile and potent tool against cancer.

1. Introduction

Cancer is one of the main causes of death worldwide and is estimated to increase in incidence and mortality in coming years (Lopes et al., 2022a; Sung et al., 2021). Aging, obesity, sedentary lifestyle, tobacco and/or alcohol consumption and exposure to different infectious, mutagenic or carcinogenic agents are some of the factors that contribute to the increase in incidence (Biemar and Foti, 2013; Arem and Loftfield, 2018; Golemis et al., 2018). The International Agency for Research on Cancer (IARC) estimates that in 2025 cancer will affect about 21.3 million people and will cause the death of 10.4 million (International Agency for Research on Cancer, Cancer Tomorrow - Estimated number of deaths for all cancers, 2024; International Agency for Research on Cancer, Cancer Tomorrow - Estimated number of new cases of all cancers, 2024). In recent years, the scientific community has made significant efforts to increase knowledge about the biology, etiology,

* Corresponding authors at: Research Institute for Medicines (iMed.ULisboa), Faculty of Pharmacy, Universidade de Lisboa, Av. Professor Gama Pinto, Lisboa 1649-003, Portugal.
E-mail addresses: mgaspar@ff.ulisboa.pt (M.M. Gaspar), catarinareis@ff.ulisboa.pt (C.P. Reis).

https://doi.org/10.1016/j.ijpharm.2024.124952
Received 5 August 2024; Received in revised form 5 November 2024; Accepted 11 November 2024
Available online 14 November 2024

prevention, diagnosis and treatment of different types of cancer (Piña-Sánchez et al., 2021).

Melanoma is a complex malignant disease that originates from melanin-producing cells, the melanocytes, and although it can develop in other areas of the body, such as the eye, ear, mucous membranes or central nervous system, it is predominantly cutaneous (Lopes et al., 2022b). Furthermore, and besides not being the most prevalent type of skin cancer, it is one of the most aggressive and consequently fatal forms among all skin cancer types (Lopes et al., 2022b; Naik, 2021; Patel et al., 2021). Concerning its treatment, and despite the irrefutable progress, the therapeutic strategies currently available in the clinic for melanoma (*i.e.*, surgery, chemotherapy, radiotherapy, immunotherapy or targeted therapy) still present challenges in terms of resistance and significant adverse effects in many cases (Ernst and Giubellino, 2022; Lopes et al., 2022a,b). Thus, exploring less invasive and more targeted, safe and effective therapeutic options remains crucial.

In this context, photothermal therapy (PTT) has been attracting the interest of many researchers as it is non-invasive, simple and precise, with few significant adverse effects, thus enabling a faster recovery of the patient (Zhao et al., 2021). PTT is based on increasing the temperature at the tumor site to induce cell death, taking advantage of the use of photothermal agents that efficiently transform the light energy received from the laser into thermal energy (Han and Choi, 2021; Lopes et al., 2022a). In the tumor environment, the accelerated rate of angiogenesis results in the formation of an immature and aberrant vasculature, leading to low levels of blood flow that favor energy and oxygen deprivation, thus making cancer cells more sensitive to heat when compared to healthy ones (Han and Choi, 2021; Hannon et al., 2021; Imashiro et al., 2021). Furthermore, PTT can be combined with other therapeutic options, such as radiotherapy, chemotherapy or immunotherapy, exploring the advantages and compensating for the limitations of each one, while also taking advantage of their synergism to maximize therapeutic efficacy (Han and Choi, 2021; Hannon et al., 2021; Logghe et al., 2024; Lin et al., 2023). Several studies have even investigated the potential of PTT in inhibiting the metastasis of various types of cancer, such as melanoma or breast cancer (Jin et al., 2013; Xie et al., 2011).

Among the physicochemical and optical characteristics of gold nanoparticles (AuNPs), the tunable surface plasmon resonance (SPR), which is responsible for the conversion of light energy into thermal energy, stands out. These properties have been widely exploited as photothermal enhancers in PTT (Lopes et al., 2023). Moreover, it is particularly interesting to use a laser with an emission wavelength in the near-infrared (NIR) region of the therapeutic optical window, where lower tissue absorption of light results in greater depth (Lopes et al., 2023; Ferreira-Gonçalves et al., 2022). Despite this, the penetration depth is limited up to 10 mm (Kaub and Schmitz, 2022; Li et al., 2021), making PTT most suitable to superficial and localized tumors such as the case of melanoma. It is important to highlight that, in addition to PTT, AuNPs have been used in various anticancer therapeutic options, such as radiotherapy (Piccolo et al., 2022; Martins et al., 2024; Schuemann et al., 2016), radiofrequency therapy (Sztandera et al., 2019), sonodynamic therapy (Wang et al., 2024; Shanei and Akbari-Zadeh, 2019) as well as carriers for cytotoxic compounds, photosensitizing agents and nucleic acids for use in chemotherapy, photodynamic therapy and gene therapy, respectively (Sztandera et al., 2019).

In this context, our group aimed to develop a formulation of AuNPs that eliminates commonly used cytotoxic reagents, opting instead for more biocompatible alternatives. We initially used an aqueous extract of *Plectranthus saccatus* Benth as a reducing agent (Silva et al., 2016). However, due to variability in its composition, we replaced it with rosmarinic acid, the major compound of the extract (Lopes et al., 2023). This formulation was then coated with a mixture of hyaluronic (HA) and oleic (OA) acids (HAOA-AuNPs) and characterized in terms of its physicochemical properties and morphology. The safety of these AuNPs in the absence of laser irradiation was validated through *in vitro* assays using different immortalized human cell lines, including healthy keratinocytes (HaCat), as well as a 3D reconstructed skin model. Additionally, *ex vivo* studies were conducted on human red blood cells and *in vivo* safety was evaluated using *Artemia salina* and healthy rodent models (Lopes et al., 2023). The present work aimed to assess, for the first time, the *in vitro* and *in vivo* efficacy profile of this nanoformulation in combination with NIR-laser irradiation, specifically focusing on its mechanism of action in melanoma cell lines (Fig. 1).

2. Materials and methods

2.1. Materials

2.1.1. Reagents

Gold (III) chloride trihydrate ($HAuCl_4 \cdot 3H_2O$), silver nitrate ($AgNO_3$), L-ascorbic acid (L-AA), rosmarinic acid (RA), hyaluronic acid (HA) sodium salt from *Streptococcus equi*, oleic acid (OA), propidium iodide (PI) and RNAse A were purchased from Sigma-Aldrich (St. Louis, Missouri, USA). Annexin V-CF647 was acquired from Merck (Rahway, Nova Jersey, USA). All other reagents were of analytical purity grade and the water purified through a Millipore system (18.2 MΩ·cm at 25 °C; Millipore, Burlington, Massachusetts, USA).

2.1.2. Cell lines and cell culture

In vitro two-dimensional (2D) assays of uncoated and HAOA-AuNPs were assessed in a murine and human melanoma cell lines, namely B16F10 (ATCC® CRL-6475™) and A375 (ATCC® CRL-1619™), respectively. Both cell lines were grown in Dulbecco's modified Eagle medium (DMEM) with high glucose (4500 mg/L) and supplemented with 10 % of Fetal Bovine Serum (FBS), 100 IU/mL of penicillin and 100 μg/mL of streptomycin, denominated complete medium.

On the other hand, the *in vitro* three-dimensional (3D) model of reconstructed human skin to evaluate the safety of laser *per se* was established using two primary cell lines, namely: Human Dermal Fibroblasts isolated from neonatal foreskin (HDFns) and Human Epidermal Keratinocytes isolated from neonatal foreskin (HEKns) (Thermofisher Scientific Inc, MA, USA). HDFns were grown in DMEM supplemented with 10 % of FBS and 2 mM of L-alanyl-l-glutamine dipeptide. HEKns were cultured in EpiLife medium supplemented with 1 % of a commercial mix of human keratinocyte growth factors and 0.06 mM of calcium chloride. Additionally, both cell lines were supplemented with 1 % of penicillin and streptomycin.

All cell lines were maintained in a humidified atmosphere of 37 °C and 5 % CO_2 and observed every 2–3 days until they reached a confluency of about 80 %.

2.1.3. Animals

C57BL/6 mice (8–10 weeks old) were acquired from Charles River (Barcelona, Spain). The animals were housed in ventilated cages under adequate hygienic conditions with a cycle of light/dark of 12 h, temperature of about 20–24 °C and relative humidity of 50–65 %. Moreover, the animals had free access to a sterilized diet and acidified water. Animal studies were carried out in agreement with the animal welfare organ (ORBEA) of the Faculty of Pharmacy of the University of Lisbon, approved by the competent national authority Direção Geral de Alimentação e Veterinária (DGAV) and in accordance with the national (DR 113/2013, 2880/2015, 260/2016 and 1/2019) and European (2010/63/EU) legislation for the use and care of animals in research.

2.2. Methods

2.2.1. Preparation of uncoated and HAOA-AuNPs

Uncoated and HAOA-AuNPs formulations were prepared according to our previously published work (Lopes et al., 2023). Briefly, for uncoated AuNPs, fresh solutions of $AgNO_3$ (1 mM), L-AA (2 mM) and RA (3.5 mM) were added to a solution of $HAuCl_4 \cdot 3H_2O$ (1 mM), at room

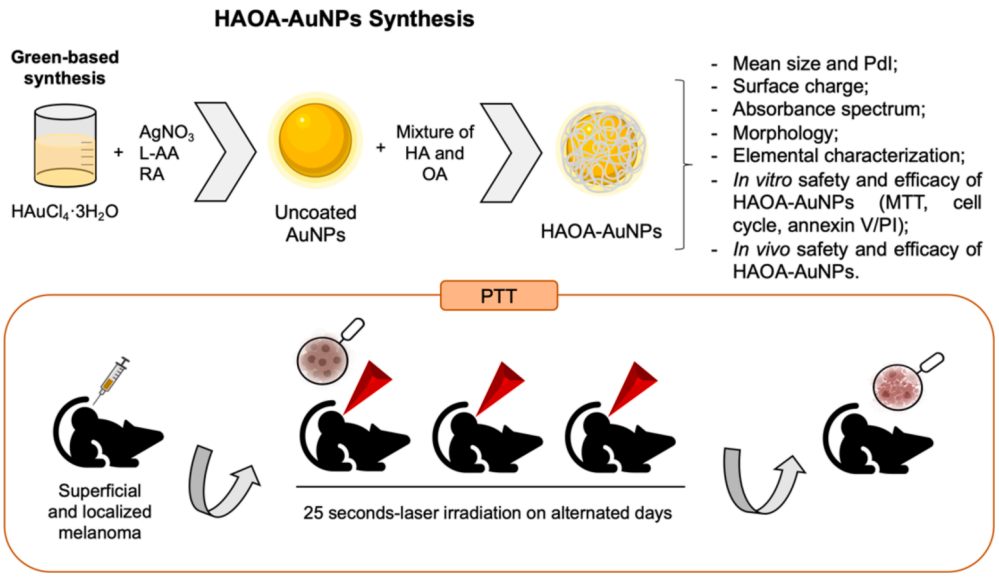

Fig. 1. Schematic representation of the preparation of HAOA-AuNPs and their anti-tumor mechanism.

temperature and under magnetic stirring at 800 rpm for 15 min. The resulting suspension was stored overnight at 4 °C and on the next day centrifuged at 1520 × *g* for 20 min (Eppendorf® Centrifuge 5804R, Hamburg, Germany) and the pellet suspended in milli-Q water. Afterwards, uncoated AuNPs were coated with a mixture of hyaluronic and oleic acids (HAOA) by mixing equal volumes of both under stirring at 800 rpm for 30 min. HAOA coating was prepared in advance by mixing 50 mg of HA with 200 μL of OA. On the following day, HAOA-AuNPs were centrifuged at 7200 × *g* for 15 min and the pellet suspended in intended volume to proceed for *in vitro* or *in vivo* assays.

It is important to note that the concentrations of both formulations mentioned throughout this article were evaluated by Inductively Coupled Plasma (ICP-OES, Ultima, Horiba Jobin-Yvon, Longjumeau, France), which measures the photon count for each gold atom and ion. The obtained intensity was then converted into mg of gold atoms and ions per liter of solution, using a calibration curve established with a standard gold solution. The linearity of the calibration curve was guaranteed from 0 to 100 mg/L ($R^2 = 0.9999$; Slope: 58,741 and y-intercept [x = 0]: 10288). Subsequently, the gold concentration in mg/L was converted to micromolar concentration using the molar mass of gold (196.967 g/mol).

2.2.2. Physicochemical characterization of uncoated and HAOA-AuNPs

The synthetized AuNPs were characterized in terms of mean size, polydispersity index (PdI), surface charge and absorbance spectrum. Mean size, determined as hydrodynamic diameter, and PdI were assessed through dynamic light scattering (DLS) (Zetasizer Nano S, Malvern Instruments, Malvern, UK) under a temperature of 25 °C and a scattering angle of 173°, by diluting the formulations in Milli-Q water (1:10, *v/v*). In its turn, the zeta potential was determined diluting the samples in PBS pH 7.4 (1:10, *v/v*) using the electrophoretic mobility technique (Zetasizer Nano Z, Malvern Instruments, Malvern, UK) at a constant temperature of 25 °C. Absorbance spectra of formulations were evaluated by UV–visible spectrophotometry (Varioskan Lux, Thermo Fisher Scientific, Waltham, MA, USA).

The stability of HAOA-AuNPs in water, their preparation and storage conditions, was evaluated after 1 month of storage at 4 °C and room temperature. Furthermore, since PBS was used as the dispersion medium for *in vivo* administration of the HAOA-AuNPs, their stability in PBS was also assessed. The results are shown in Supplementary Material (Figure S1).

2.2.3. Morphological and elemental characterization of uncoated and HAOA-AuNPs

The morphological and elemental characterization of synthesized uncoated and HAOA-AuNPs was carried out by Scanning Electron Microscopy (SEM) and Energy dispersive X-ray spectroscopy (EDS), respectively. For that, one drop of each AuNPs suspension was put on a silicon substrate and allowed to dry for some minutes. Images were acquired throughout a Hitachi Regulus 8220 Scanning Electron Microscope (Hitachi, Mito, Japan) coupled with an Oxford EDS detector (Oxford Instruments, Abingdon, Oxfordshire, England).

2.2.4. Irradiation procedures

In vitro efficacy, cell cycle and Annexin V/PI assays were performed with a Fiber-Coupled Laser System (FC-808–2 W, Frankfurt Laser Company, Friedrichsdorf, Hessen Germany) coupled to an FPYL-COL-X collimator (Frankfurt Laser Company, Friedrichsdorf, Hessen Germany) emitting at a wavelength of 808 nm and using an irradiance of 9.2 W/cm^2 for 5 min, corresponding to a dose of 27.6 J/mm^2. Henceforward, these irradiation conditions were denominated as irradiation condition (1).

For *in vitro* 3D reconstructed human skin model and due to the larger diameter of the inserts, the non-colimated Roithner Lasertechnik GmbH laser (RLTMDL-808–5 W-5, Vienna, Austria) emitting at a wavelength of 808 nm was used. The irradiation dose of 27.6 J/mm^2 tested in all previous *in vitro* assays was maintained and will be designated as irradiation condition (2).

The *in vivo* assays were conducted with the previously mentioned equipment, Roithner Lasertechnik GmbH (RLTMDL-808–5 W-5, Vienna, Austria), emitting at a wavelength of 808 nm and using an irradiance of 0.94 W/cm^2. Henceforth, these irradiation conditions were mentioned as irradiation condition (3).

2.2.5. In vitro efficacy assessment of uncoated and HAOA-AuNPs

In vitro efficacy of uncoated and HAOA-AuNPs after laser irradiation was evaluated in murine and human melanoma cell lines, B16F10 and A375, respectively, by the 3-(4,5-dimethylthiazol-2-yl)-2,5-diphenyltetrazolium bromide (MTT) assay (Lopes et al., 2020; Pinho et al., 2023). Both cell lines were seeded in septuplicate *per* sample in a 96-well plate at a concentration of 5 × 10^4 cells/mL and allowed to adhere overnight. On the next day, the medium was replaced by fresh complete medium containing uncoated or HAOA-AuNPs at different concentrations (100, 200 and 400 μM in terms of gold content) for 4 h. Cells incubated with

complete medium were used as a negative control. Thus, after incubation time and with the aim of eliminating the unbound and not uptaken AuNPs, the supernatant from each well was removed and replaced by 100 μL of fresh complete medium to proceed to irradiation procedures. These assays were performed according to irradiation condition (1). Twenty-four hours after, supernatant was removed, and cells were washed twice with PBS at pH 7.4. Afterwards, 50 μL MTT solution (0.5 mg/mL) was added to each well and plates were incubated for a period of 2–3 h at 37 °C and under a 5 % CO_2 atmosphere. Finally, to solubilize the crystals of formazan formed, 200 μL of DMSO was added and the absorbance at 570 nm was measured in a microplate reader (BioTekTM EL × 800^{TM} Absorbance Microplate Reader, BioTek Instruments, Inc., Winooski, VT, USA). The percentage of viable cells was determined in relation to the negative control, according to equation (1):

$$\text{Cell viability}\,(\%) = \frac{\text{Abs}_{\text{sample}}}{\text{Abs}_{\text{negative control}}} \times 100 \quad (1)$$

where $\text{Abs}_{\text{sample}}$ is the absorbance of the sample and $\text{Abs}_{\text{negative control}}$ the absorbance of cells exposed only to complete medium.

2.2.6. In vitro evaluation of cellular uptake of uncoated and HAOA-AuNPs

The *in vitro* evaluation of cellular uptake of uncoated and HAOA-AuNPs in B16F10 and A375 melanoma cell lines was performed based on the method described by Lin and coworkers (Xie et al., 2017). Briefly, B16F10 and A375 cells were seeded in a 24-well plate at a density of 5 × 10^4 cells/mL and allowed to adhere overnight. On the next day, the medium was replaced by 1 mL of fresh medium containing uncoated or HAOA-AuNPs at a concentration of 200 μM in terms of gold content. After 4 h of incubation, the supernatant of each well was removed, and the cells were washed twice with 0.5 mL of PBS. Finally, the cells were harvested with TrypLE™ and centrifuged at 1000 × *g* for 5 min and the supernatant discarded. Cells were digested with 0.5 mL of fresh *aqua regia* (HNO_3: HCl (1:3 *v/v*)) for 10 min and diluted to a total volume of 1 mL with milli-Q water. The gold concentration in cells was determined by ICP-OES and represented as cellular uptake of AuNPs in percentage of total dose.

2.2.7. Elucidating the mechanisms of action of HAOA-AuNPs in combination with laser

The mechanism of cell death associated to PTT in combination with the HAOA-AuNPs was evaluated using two different flow cytometry methodologies, namely, cell cycle and Annexin V/PI assays using B16F10 and A375 melanoma cell lines.

2.2.7.1. Cell cycle assay. For cell cycle analysis, melanoma cells were seeded in septuplicate *per* sample in a 96-well plate at a concentration of 7 × 10^4 cells/mL and allowed to adhere overnight at 37 °C and 5 % CO_2. On the next day, the medium was replaced by fresh one containing the most promising formulation, HAOA-AuNPs, at 200 μM and the plates incubated for 4 h. At the end of the incubation period, the supernatant was removed and replaced by 100 μL of fresh complete medium. As described in section 2.2.4., samples were submitted to laser irradiation, condition (1). Twenty-four hours after irradiation, supernatants were discarded, and adherent cells were harvested with TrypLE™ and centrifuged at 800 × g for 5 min at 4 °C. The supernatants were discarded, and the pellet suspended firstly in ice-cold PBS (500 μL) and then fixed under gentle agitation with ice-cold 80 % ethanol (500 μL) added drop-by-drop. Finally, samples were kept at 4 °C for at least 16 h prior to analysis. On the day of data collection, samples were centrifuged (850 × *g*, 5 min, 4 °C) and suspended in a PBS solution containing 25 μg/mL of PI and 50 μg/mL of RNase A and incubated at 37 °C for 30 min (Pinho et al., 2023; Pinho et al., 2023). The Guava easyCyte^{TM} Flow Cytometer (Merck Millipore, Darmstadt, Germany) was used to sample acquisition, counting 10.000 events *per* sample. Data were analyzed using the ModFit LT^{TM} 6.0 software (Verity Software House, Topsham, ME, USA).

2.2.7.2. Annexin V/PI assay. For the Annexin V-CF647/PI assay, a similar methodology to that described above for cell cycle up to and including the irradiation procedure stage was performed. Twenty-four hours after irradiation, floating and adherent cells were collected and centrifuged at 650 × g for 5 min. Then, the pellet was suspended in a solution containing the Annexin V (80 × diluted for both cell lines) and incubated for 15 min in a CO_2 incubator at 37 °C. Afterwards, the samples were centrifuged once again (650 × g, 5 min) before adding the PI solution at a concentration of 0.1 μg/mL for both cell lines. The acquisition of samples was performed in full-spectrum cytometer Cytek® Aurora (Cytek Biosciences, Fremont, California) counting 50.000 events *per* sample. Data analysis was performed using FCS ExpressTM software, version 7.20.0020 (DeNovo Software). Details about gating strategy for apoptosis analysis by flow cytometry can be found in the Supplementary Material (Figure S3).

2.2.8. In vitro 3D skin model

To confirm the safety of laser irradiation, the same dose used in previous *in vitro* 2D efficacy assays was tested according to irradiation condition (2) in an *in vitro* 3D model of reconstructed human skin. The model was developed in accordance with previously published protocols (Hipólito et al., 2024; Hall et al., 2022; Zoio et al., 2021). Briefly, porous polystyrene scaffolds (Alvetex®, AVP005-48, REPROCELL Europe, Glasgow, UK) were placed in 6-well plates, immersed for 30 min in a 70 % ethanol solution to give them hydrophilic characteristics and finally washed twice with PBS. Next, 2 x 10^6 HDFns cells in 100 μL of fibroblast growth medium were plated in the upper compartment of the scaffold and incubated for 1.5 h in an atmosphere of 37 °C with 5 % CO_2 to allow adhesion of the cells. After this time, each scaffold was submerged with 9 mL of fibroblast growth medium supplemented with L-ascorbic acid (100 μg/mL) and plates were again incubated under the same conditions mentioned above and the medium renewed every 5 days for two weeks. On the 15th day, 1 × 10^6 HEKns cells in 100 μL of keratinocyte growth medium were seeded in the upper compartment of each scaffold and 3 days after the system was exposed to the air–liquid interface by removing the existing medium. In the plate compartment, the culture medium was replaced with keratinocyte growth medium supplemented with calcium chloride (1.5 mM), keratinocyte growth factor (10 ng/μL) and L-ascorbic acid (50 μg/mL). Medium replacement was performed every 2 days for 18 days to allow HEKn cells differentiation in the different strata of the epidermis On the 19th day, the scaffolds were subjected to laser according to irradiation condition (2) and after 48 h, the scaffolds were fixed in 10 % formalin solution for subsequent histological analysis by Haemotoxylin and Eosin (H&E) and anti-Cytokeratin AE1 and AE3 immunohistochemistry staining.

2.2.9. In vivo studies

2.2.9.1. Safety assessment of laser irradiation. Before evaluating the anti-tumor efficacy, the safety of the laser irradiation was performed. The main objective was to select the best experimental conditions, avoiding any injury/burn in the irradiated area of healthy mice. For this, twenty-one healthy C57BL/6 mice were shaved on their back and divided into 7 groups. Due to their black fur, an irradiance lower than the one used in *in vitro* models was tested. Thus, all animals were exposed to an irradiance of 0.94 W/cm^2 of NIR-laser for 10, 15, 20, 25, 30, 35 or 40 s. *In vivo* irradiation procedures were performed according to irradiation condition (3). Twenty-four hours after laser irradiation, the animals were sacrificed and the portion of skin irradiated by the laser was collected and fixed in a 10 % formalin solution for histological analysis. Samples were examined using a CX21 microscope (Olympus Corporation, Tokyo, Japan) and images were obtained with the NanoZoomer-SQ Digital slide scanner C13140-01 (Hamamatsu

Photonics, Shizuoka, Japan). Representative images were taken using the NDP.view2 Image viewing software (Hamamatsu Photonics, Shizuoka, Japan).

2.2.9.2. Efficacy assessment of PTT using HAOA-AuNPs. For these studies, C57BL/6 mice were selected for the establishment of the subcutaneous melanoma syngeneic model. For tumor induction, a total of 1.3×10^5 B16F10 murine melanoma cells were suspended in PBS pH 7.4 (100 μL) and injected subcutaneously in the right flank of mice previously shaved. The animals and the size of tumors were monitored until reaching a palpable mean size of about 200–400 mm^3 (around 10 days) and the therapeutic protocol started (day 0). For this study, the animals were randomly distributed into four groups: 1) negative control (induced and non-treated); 2) animals exposed to laser irradiation for 25 s; 3) animals that received a single intratumoral administration of HAOA-AuNPs (3.1 mg Au/Kg body weight) and 4) animals that received a single intratumoral administration of HAOA-AuNPs (3.1 mg Au/Kg body weight) and 4 h after injection, exposed to laser irradiation for 25 s (Fig. 2).

Animals without tumor (naïve) were also included in the study. Animals from groups 2 and 4 received three laser irradiations of 25 s each on days 0, 2 and 4. As in the previous laser safety section, all laser procedures were performed according to irradiation condition (3).

The selected irradiation conditions were based on the results of the laser safety assay on healthy C57BL/6 mice (0.94 W/cm^2, 25 s; corresponding to a dose of 24 J/cm^2). The tumor volume of all animals was regularly recorded using a digital caliper on days 0, 2 and 4 and calculated according to the formula 2 (Pinho et al., 2023).

$$\text{Tumor volume}\,(mm^3) = \frac{L \times W^2}{2} \quad (2)$$

where L and W is the longest and shortest axis of the tumor, respectively.

Twenty-four hours after the last irradiation exposure, mice were sacrificed and blood collected for determination of plasmatic levels of hepatic biomarkers, namely aspartate aminotransferase (AST) and alanine aminotransferase (ALT). Moreover, metabolic and elimination organs such as liver, kidneys and spleen, were excised and accurately weighted to determine its tissue index according to the formula 3 (Matos et al., 2022).

$$\text{Tissue index} = \sqrt{\frac{\text{organ weight}}{\text{animal weight}} \times 100} \quad (3)$$

Then, the organs were fixed in a 10 % formalin solution to histological analysis and processed for routine analysis with H&E staining. Slides were analyzed with a CX21 microscope (Olympus Corporation, Tokyo, Japan) and images were acquired with the NanoZoomer-SQ Digital slide scanner C13140-01 (Hamamatsu Photonics, Shizuoka, Japan). Representative images were taken using the NDP.view2 Image viewing software (Hamamatsu Photonics, Shizuoka, Japan).

The collected blood, organs and tumors were also used to quantify gold content at the end of the experimental protocol in the animals subjected to intratumoral administration of HAOA-AuNPs. Gold quantification was performed by ICP-OES. Samples were frozen, lyophilized and finally micronized and homogenized by crushing. The totality of that mass in the case of the blood and spleen or a part of that mass in the larger organs such as liver and kidneys was subjected to a microwave digestion process using a mixture of nitric acid and hydrochloric acid (HCl: HNO_3 (3:1 *v/v*)) and two heating ramps (120 °C for 5 min, followed by 180 °C for 5 min). The resulting solution of this process was slightly orange but completely clear. The solution was diluted for a final volume of 5 mL and gold content was quantified.

2.2.10. Statistical analysis

In vitro results were expressed as mean ± standard deviation (SD) of at least three independent experiments. *In vivo* results were expressed as mean ± standard error of mean (SEM) of at least three animals *per* group. Statistical analysis was performed using the GraphPad Prism 9® (GraphPad Software Inc., Boston, Massachusetts, USA) and a *p-value* < 0.05 was considered as statistically significant.

3. Results

3.1. Physicochemical characterization of uncoated and HAOA-AuNPs

In a previous work, a formulation of uncoated AuNPs and its coating with a mixuture of hyaluronic and oleic acid (HAOA-AuNPs) were optimized and have demonstrated to be safe in *in vitro*, *ex vivo* and *in vivo* models (Lopes et al., 2023). Following this initial safety study, we aimed to evaluate their *in vitro* and *in vivo* efficacy in combination with NIR laser irradiation. The physicochemical properties of uncoated and HAOA-AuNPs used throughout this study, namely, mean size, polydispersity index, zeta potential and absorbance spectra are depicted in Fig. 3.

Higher values of mean size were observed for coated AuNPs (109 *vs.* 78 nm). In case of PdI, a reduction of this value was also achieved after coating (0.415 *vs.* 0.261). Both AuNPs exhibited negative surface charge; HAOA-AuNPs presented a more negative zeta potential due to the presence of hyaluronic acid at the external surface. In turn, the most important feature was the fact that the absorbance at 808 nm, crucial for the application of PTT, was enhanced with the addition of the coating.

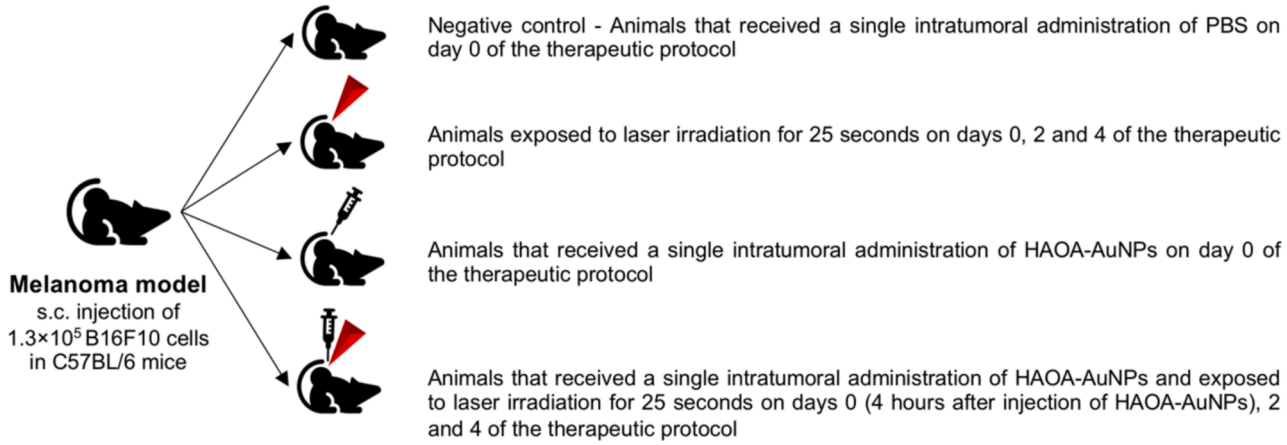

Fig. 2. Illustrative representation of the different groups for the efficacy assessment of PTT using HAOA-AuNPs.

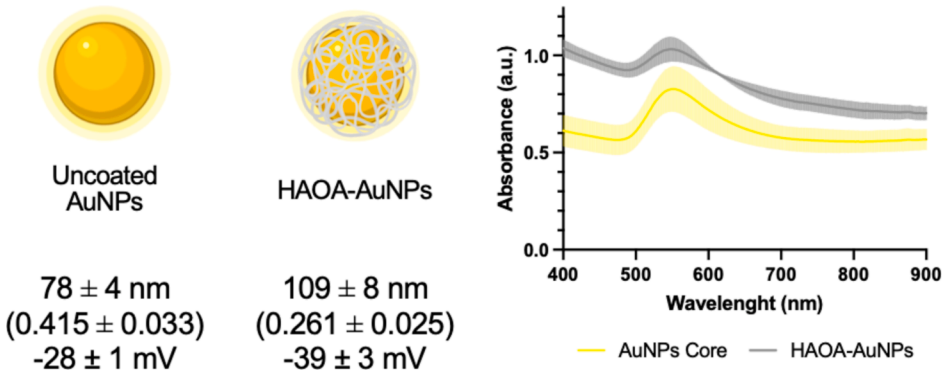

Fig. 3. Mean size (hydrodynamic diameter, nm), polydispersity index (PdI), surface charge (zeta potential, mV) and absorbance spectra of uncoated and HAOA-AuNPs at syntheses concentration. Data are presented as mean value ± SD, n ≥ 3.

3.2. Morphological and elemental characterization of uncoated and HAOA-AuNPs

The morphology of uncoated and HAOA-AuNPs was assessed by SEM and it is shown in Fig. 4. The analysis of the images showed that the formulation of uncoated AuNPs presented three subpopulations: quasi-spherical AuNPs of smaller size, between 50 and 80 nm; a nanoflower morphology resembling agglomeration of smaller AuNPs and planar AuNPs with variable shapes and sizes. Moreover, we also concluded that the coating did not interfere with their morphology, as we observed the same type of nanoparticles but with a visible coating layer.

In addition, the elemental composition of the produced AuNPs was performed by combined SEM-EDS analysis (Fig. 5). The results clearly confirmed the gold content in both AuNPs formulations.

3.3. In vitro efficacy assessment of uncoated and HAOA-AuNPs

The safety of AuNPs and laser irradiation alone as well as the efficacy of their combination were tested *in vitro* in B16F10 and A375 melanoma cell lines, using the MTT assay. For this, the uncoated and HAOA-AuNPs at three different concentrations (100, 200 and 400 μM) were added to cells for 4 h. After this period, and before laser irradiation, the cell medium was renewed to eliminate AuNPs that had not been internalized by the cells. The results are depicted in Fig. 6, 24 h after irradiation condition (1). The selection of the concentration range was based on previous safety results of these formulations tested in different healthy and cancer human cell lines up to a concentration in terms of gold of 600 μM (Lopes et al., 2023).

It was clear that laser irradiation alone, *i.e.* without AuNPs (no treatment), did not significantly affect cell viability for both cell lines. Likewise, cells incubated with uncoated or HAOA-AuNPs, in the absence of laser (white columns), and regardless of the concentration tested (100, 200 or 400 μM), showed cell viability always above 75 % (dashed line). An exception was observed for the murine cell line B16F10 with HAOA-AuNPs at the highest concentration tested (400 μM), where a cell viability value of 54 ± 3 % was obtained.

In turn, by combining AuNPs and laser irradiation (black columns), a significant decrease in cell viability was found in both cell lines 24 h after irradiation.

In B16F10 cells, the percentage of cell viability of 26 ± 5 % after laser activation was independent of the formulation and concentration of the AuNPs tested.

Conversely, in human melanoma cells, it was observed that after laser activation, cell viability significantly decreased as the concentration of AuNPs (coated or uncoated) increased. For uncoated AuNPs, viability was 72 ± 10 %, 43 ± 1 % and 23 ± 2 % for doses of 100, 200 and 400 μM, respectively. For HAOA-AuNPs, cell viability was 82 ± 10 %, 41 ± 1 % and 17 ± 1 % for doses of 100, 200 and 400 μM, respectively. It should be noted that, similarly to the murine cell line, no significant differences were detected in the percentage of cell viability achieved after laser activation between uncoated and HAOA-AuNPs in A375 cells.

3.4. In vitro evaluation of cellular uptake of uncoated and HAOA-AuNPs

The cellular uptake of uncoated and HAOA-AuNPs at a concentration of 200 μM in terms of gold content after 4 h of incubation in murine melanoma (B16F10) and human melanoma (A375) cell lines was performed by quantifying intracellular gold content using ICP-OES. As seen in Fig. 7, the percentage of internalized AuNPs after 4 h of incubation with uncoated AuNPs was 40 % for B16F10 and 54 % for A375 cells while for HAOA-AuNPs was 44 % and 49 %, respectively. Specifically, uncoated AuNPs showed a cell line-dependent pattern, being significantly more internalized by A375 cells (54 ± 4 %) compared to B16F10

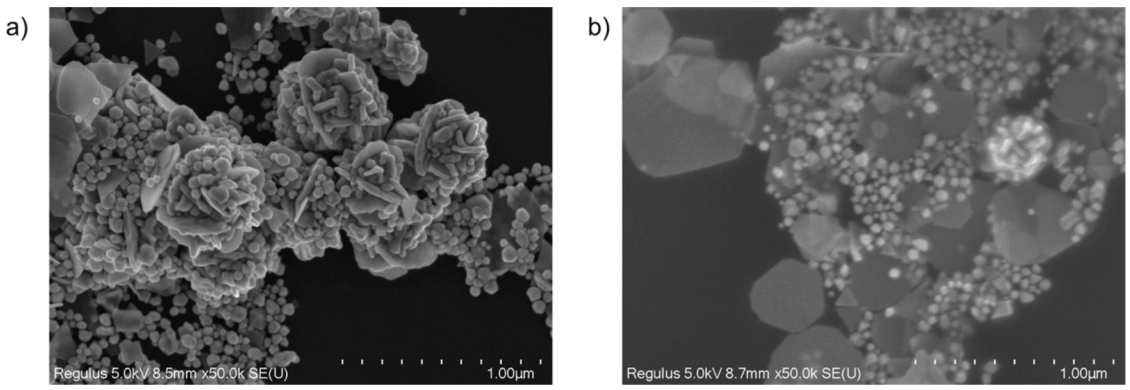

Fig. 4. Scanning electron microscopy (SEM) of uncoated (a) and HAOA-AuNPs (b).

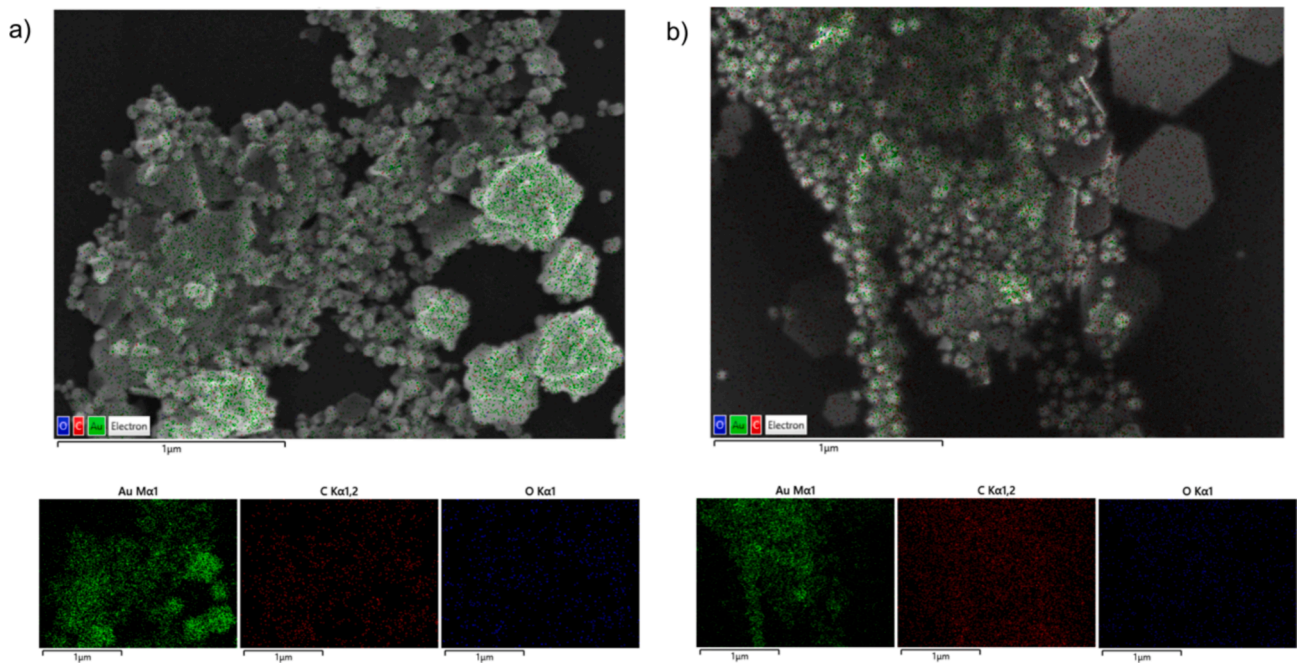

Fig. 5. EDS layered image of uncoated (a) and HAOA-AuNPs (b), confirming the high presence of gold content.

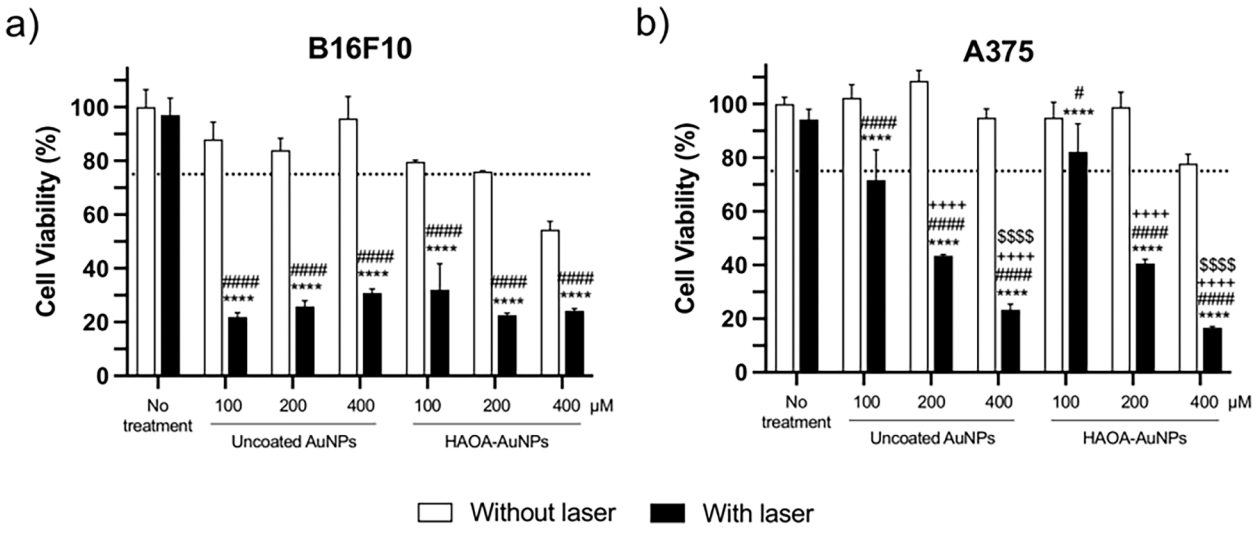

Fig. 6. Cell viability (%) of B16F10 (a) and A375 (b) cell lines 24 h after incubation with uncoated and HAOA-AuNPs at three different concentrations (100, 200 and 400 µM) in the absence or presence of laser. Data are presented as mean ± SD, n ≥ 4. One-way analysis of variance (ANOVA), Šídák's test ($p < 0.05$) was used to detect differences between the groups. * $p < 0.0332$ and **** $p < 0.0001$ *vs.* no treatment without laser; #### $p < 0.0001$ *vs.* same formulation (uncoated or HAOA-AuNPs) at same concentration (100, 200 or 400 µM) without laser; ++++ $p < 0.0001$ *vs.* same formulation at a concentration of 100 µM; $$$$ $p < 0.0001$ *vs.* same formulation at a concentration of 200 µM.

cells (40 ± 5 %).

3.5. Elucidating the mechanisms of action of HAOA-AuNPs in combination with laser

The combinatorial effect of HAOA-AuNPs and laser irradiation on cell cycle progression was evaluated in B16F10 and A375 cell lines (Figs. 8 and 9, respectively). HAOA-AuNPs were tested at a concentration of 200 µM and submitted to irradiation condition (1).

In general, cell cycle analysis in both melanoma cell lines revealed that the presence of HAOA-AuNPs or laser irradiation did not promote alterations in the cell cycle in comparison with untreated cells (control). On the contrary, the combined therapy of HAOA-AuNPs with laser resulted in significant changes in the cell cycle.

In B16F10 cells, the cell cycle analysis revealed that the combination of HAOA-AuNPs and the laser increased the percentage of cells in S phase from 41, 43 and 42 to 53 % compared to the control, control with laser and HAOA-AuNPs without laser, respectively (Fig. 8). Furthermore, this change was associated with a reduction in the percentage of cells in the G0/G1 phase from 51, 50 and 49 to 43 % compared to control, control with laser and HAOA-AuNPs without laser, respectively. It should be noted that the percentage of cells in the G2/M phase in HAOA-AuNPs and laser also showed a decreasing trend compared to all others. The results demonstrated that the combined therapy significantly induced a S-phase cell cycle arrest in B16F10 cells.

Similarly, in A375 cells, the combination of HAOA-AuNPs and laser

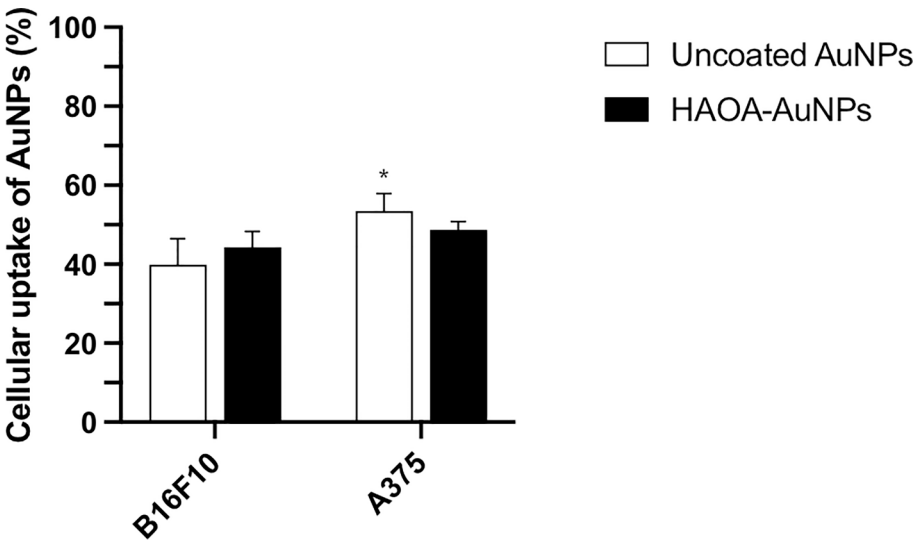

Fig. 7. Cellular uptake of uncoated and HAOA-AuNPs as a percentage of the total dose in B16F10 and A375 melanoma cell lines 4 h after incubation. Data are presented as mean ± SD, n = 3. Two-way analysis of variance (ANOVA), Šídák's test ($p < 0.05$) was used to detect differences between the groups. * $p < 0.0332$ *vs.* same formulation in B16F10 cell line.

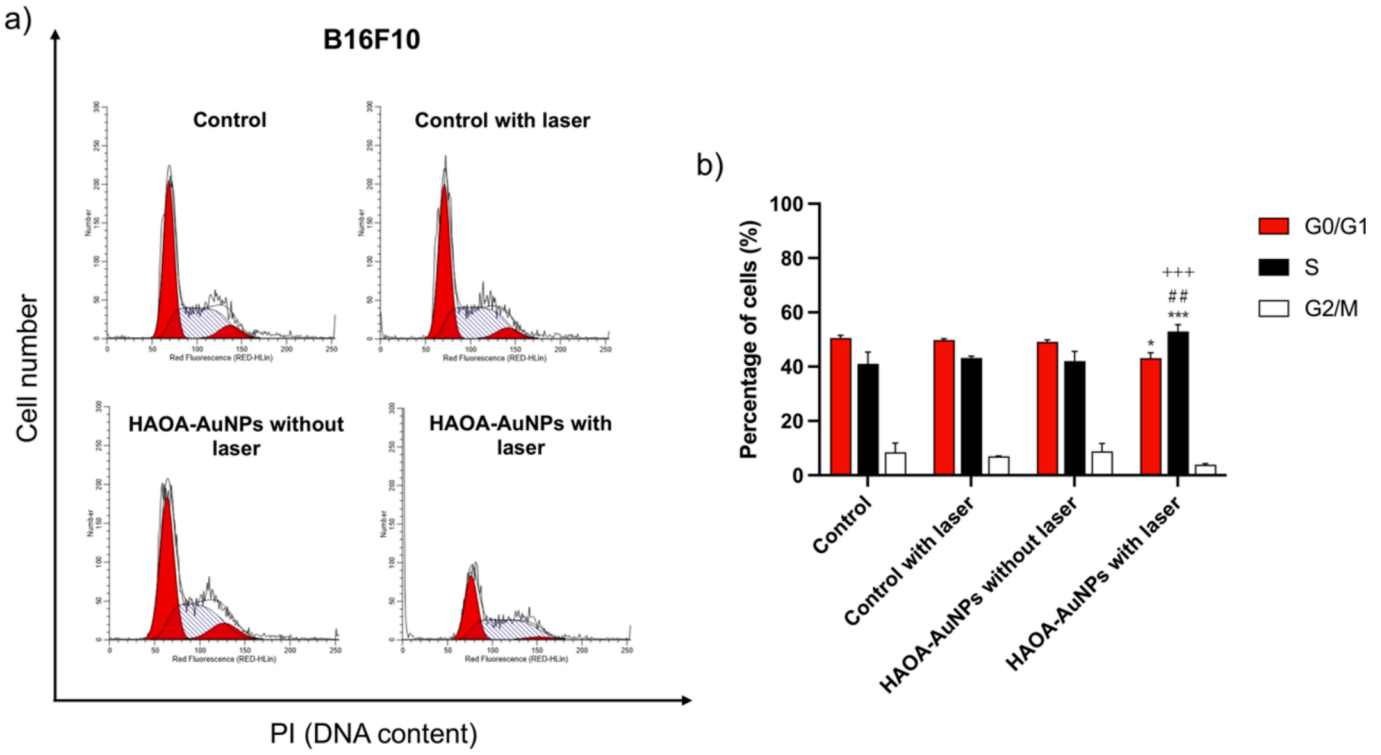

Fig. 8. Representative cell cycle histogram (a) and quantitative analysis of the distribution of the cell population in the G0/G1, S and G2/M phases of the cell cycle (b) in the B16F10 cell line in the absence of HAOA-AuNPs and laser (control), in the presence of laser (control with laser) as well as in the presence of HAOA-AuNPs at 200 μM (HAOA-AuNPs without laser) and in the combination of HAOA-AuNPs at 200 μM and laser irradiation (HAOA-AuNPs with laser). The results were obtained 24 h after irradiation. Data are presented as mean ± SD, n ≥ 3. Two-way analysis of variance (ANOVA), Tukey's test ($p < 0.05$) was used to detect differences between the groups. * $p < 0.0332$ and *** $p < 0.0002$ *vs.* control in the respective phase. $^{\#\#}$ $p < 0.0021$ *vs.* control with laser in the respective phase. $^{+++}$ $p < 0.0002$ *vs.* HAOA-AuNPs without laser in the respective phase.

irradiation increased the percentage of cells in S phase from 38 and 37 to 43 %, compared to control and control with laser or HAOA-AuNPs without laser, respectively (Fig. 9). Furthermore, this change was associated to a significantly reduction in the percentage of A375 cells in the G0/G1 phase from 58 to 46 % compared to control, control with laser and HAOA-AuNPs without laser. It should be noted that the percentage of cells in the G2/M phase in HAOA-AuNPs and laser showed an increasing trend compared to all others. The results demonstrated that combining therapy significantly induced a S-phase cell cycle arrest in A375 cells.

The mechanism of cell death associated to the combination of HAOA-AuNPs 24 h after laser irradiation was also determined by the Annexin V-CF647/PI assay in B16F10 and A375 cells (Figs. 10 and 11, respectively).

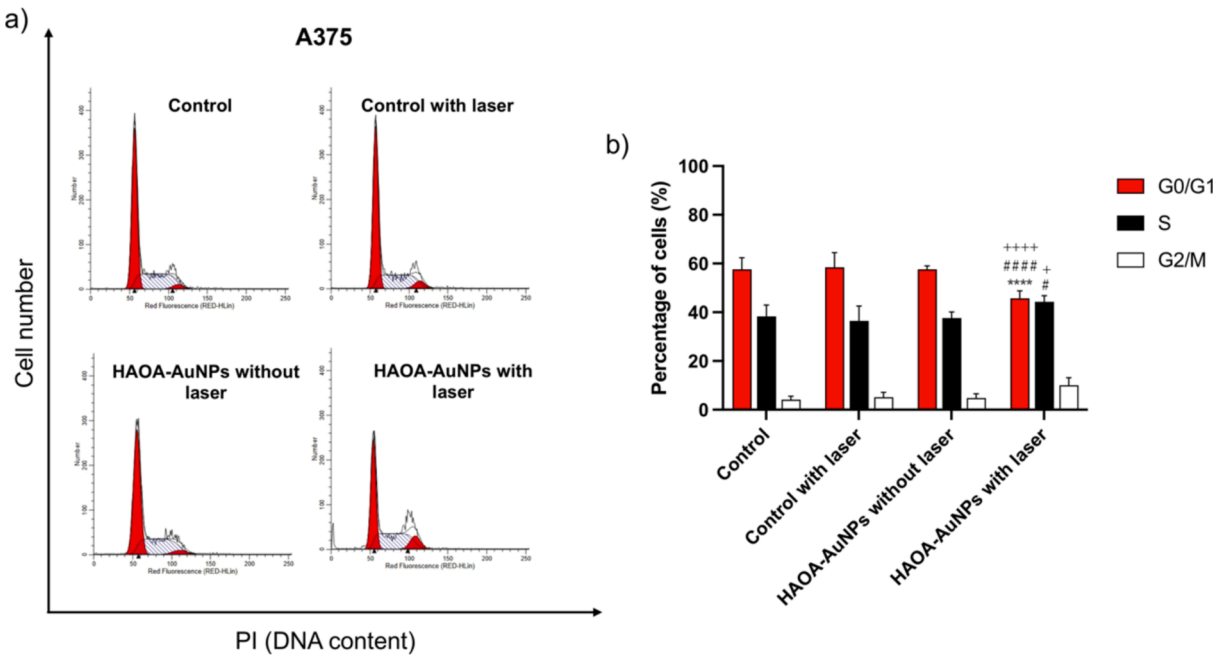

Fig. 9. Representative cell cycle histogram (a) and quantitative analysis of the distribution of the cell population in the G0/G1, S and G2/M phases of the cell cycle (b) in the A375 cell line in the absence of HAOA-AuNPs and laser (control), in the presence of laser (control with laser) as well as in the presence of HAOA-AuNPs at 200 μM (HAOA-AuNPs without laser) and in the combination of HAOA-AuNPs at 200 μM and laser irradiation (HAOA-AuNPs with laser). The results were obtained 24 h after irradiation. Data are presented as mean ± SD, n ≥ 3. Two-way analysis of variance (ANOVA), Tukey's test ($p < 0.05$) was used to detect differences between the groups. **** $p < 0.0001$ *vs.* control in the respective phase. $^{\#}$ $p < 0.0332$ and $^{\#\#\#\#}$ $p < 0.0001$ *vs.* control with laser in the respective phase. $^{+}$ $p < 0.0332$ and $^{++++}$ $p < 0.0001$ *vs.* HAOA-AuNPs without laser in the respective phase.

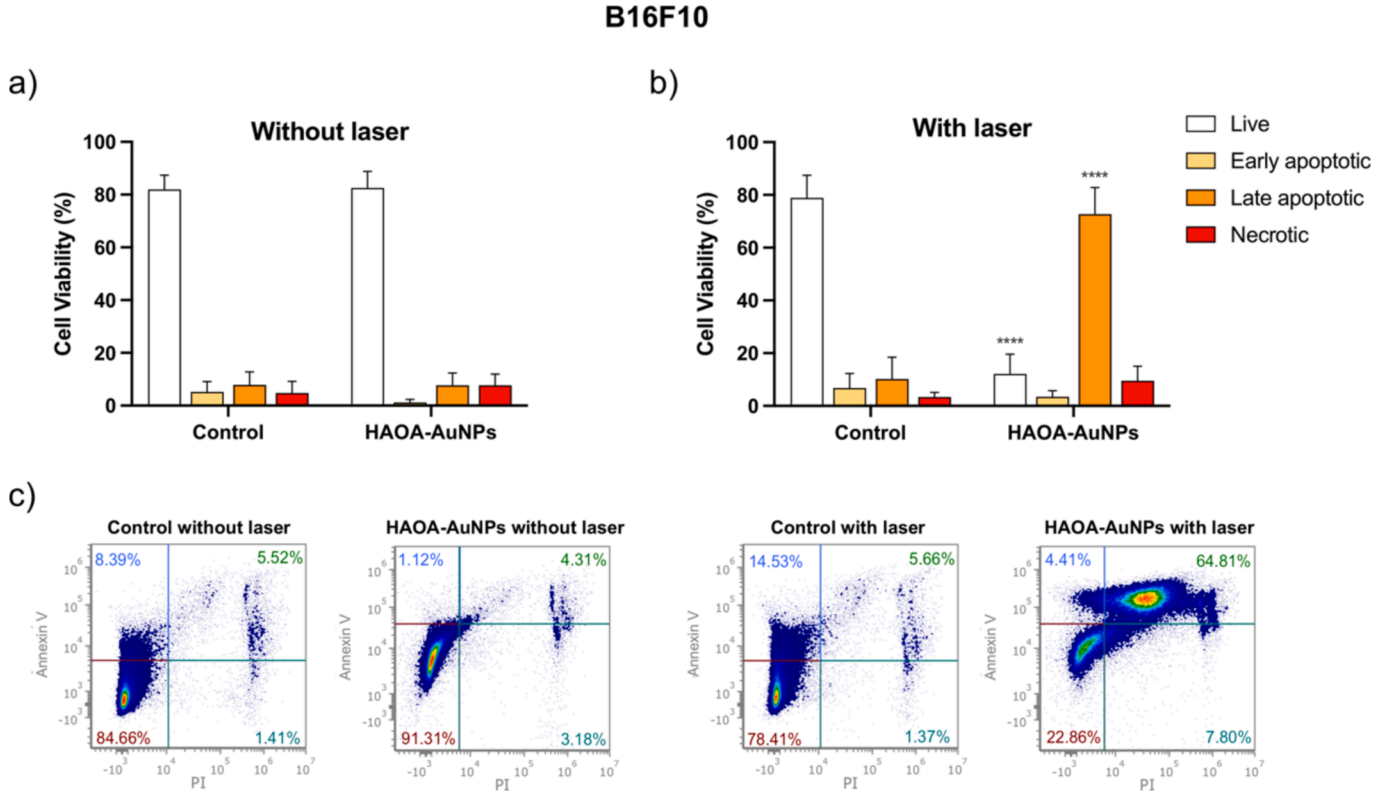

Fig. 10. Quantitative analysis of B16F10 cell population distribution at different stages (live, early apoptotic, late apoptotic and necrotic cells) in the absence (a) or presence (b) of laser irradiation without and with the presence of HAOA-AuNPs at 200 μM; and representative flow cytometry plots within all events excluding debris using Annexin V/PI staining for apoptosis (c). The results were obtained 24 h after irradiation. Data are presented as mean ± SD, n ≥ 3. Two-way analysis of variance (ANOVA), Šídák's test ($p < 0.05$) was used to detect differences between the groups. **** $p < 0.0001$ *vs.* control.

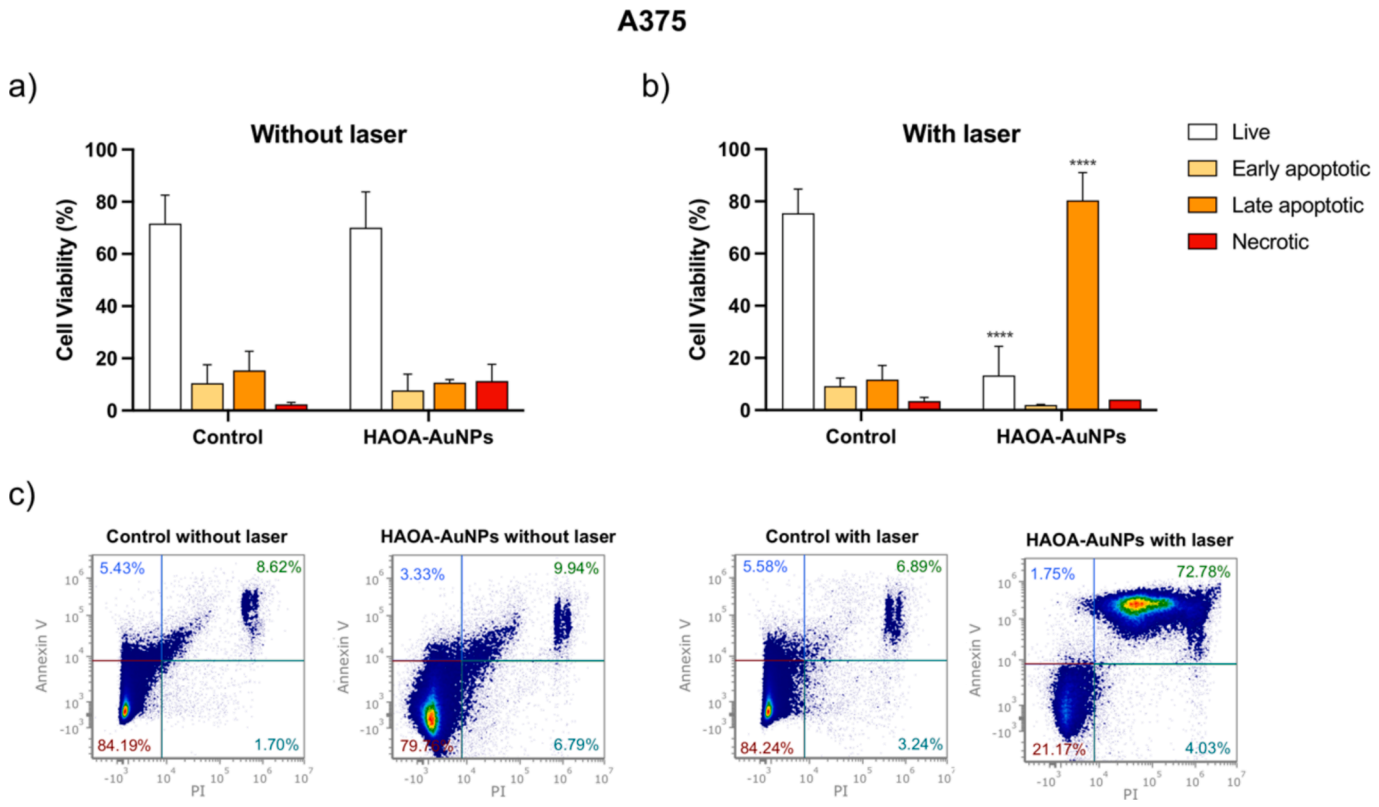

Fig. 11. Quantitative analysis of A375 cell population distribution at different stages (live, early apoptotic, late apoptotic and necrotic cells) in the absence (a) or presence (b) of laser irradiation without and with the presence of HAOA-AuNPs at 200 μM; and representative flow cytometry plots within all events excluding debris using Annexin V/PI staining for apoptosis (c). The results were obtained after a period of 24 h after irradiation. Data are presented as mean ± SD, n ≥ 3. Two-way analysis of variance (ANOVA), Šídák's test ($p < 0.05$) was used to detect differences between the groups. **** $p < 0.0001$ *vs.* control.

In the case of B16F10 cells (Fig. 10), we observed that in the absence of laser (Fig. 10a), the percentage of live cells and in early apoptosis, late apoptosis and necrosis was similar for control and cells incubated with HAOA-AuNPs at 200 μM. In contrast, after laser irradiation (Fig. 10b), the percentage of live cells decreased drastically and significantly from around 80 % in the control group with laser to around 12 % in the combined therapy (HAOA-AuNPs with laser). Concomitantly, the percentage of cells in the late apoptosis increased significantly from around 10 % in the control to a mean value of 72 % in the combined therapy. Furthermore, a positive control of apoptosis (incubation of cells at 55 °C for 20 min) was used, and more than 90 % of cells in a late apoptotic stage were achieved (data not shown).

These results revealed that for B16F10 murine melanoma cells, the combined therapy of HAOA-AuNPs with laser led to a late apoptosis, as supported by flow cytometry images representative of the different groups (Fig. 10c).

In the case of the A375 cell line (Fig. 11), similar to the observations in murine melanoma cells, no significant changes were noted in distribution percentages of cells at different stages between those treated with or without HAOA-AuNPs in absence of laser (Fig. 11a). Changes in phosphatidylserine and propidium iodide were only noticed after laser irradiation (Fig. 11b). In this case, the percentage of live cells decreased significantly from around 75 % in cells submitted to laser (control with laser) to around 13 % in the combined therapy HAOA-AuNPs with laser. In turn, the percentage of cells in the late apoptosis stage increased significantly from around 11 % in the control to a mean value of 80 % in the combined therapy group. A positive control of apoptosis led to more than 90 % of cells in the late apoptotic stage (data not shown).

Much like in B16F10 cells, these data also suggest that for the A375 cell line, the combined therapy of HAOA-AuNPs with laser resulted on a late apoptosis as supported by flow cytometry images representative of the different groups (Fig. 11c).

3.6. *In vitro 3D skin model*

To additionally confirm the safety of laser irradiation, the evaluation of its impact in an *in vitro* 3D reconstructed human skin model was performed. This model was developed over five weeks and, afterwards, it was irradiated with the same doses previously used in 2D *in vitro* efficacy assays (27.6 J/mm^2) and according to the irradiation condition (2). Representative images of both groups, without or with laser, staining with H&E and anti-Cytokeratin AE1 and AE3 immunohistochemistry are shown in Fig. 12. The structure in both samples is composed of a stratified squamous epithelium of well-differentiated keratinocytes that present progressive keratinization. Moreover, the epithelium rests on a regular and thick lamina propria of loose connective tissue, composed of a moderate number of fibroblasts and fibrocytes surrounded by a pale basophilic and amphophilic fibrillar matrix. In turn, anti-Cytokeratin AE1/AE3 immunohistochemical staining revealed the expression of high amounts of cytoplasmic cytokeratins in keratinocytes. In summary, no changes in cell morphology or tissue structure, between the control group (without laser irradiation) and the irradiated samples were observed, thus supporting the safety of laser irradiation at the tested dose.

3.7. *In vivo studies*

3.7.1. *Safety assessment of laser irradiation*

To study the *in vivo* efficacy of the combined therapy of HAOA-AuNPs with laser, we performed a prior assessment of the safety of laser irradiation alone in an *in vivo* context. For this, twenty-one healthy C57BL/6 mice with shaved backs were divided into 7 groups for 10, 15,

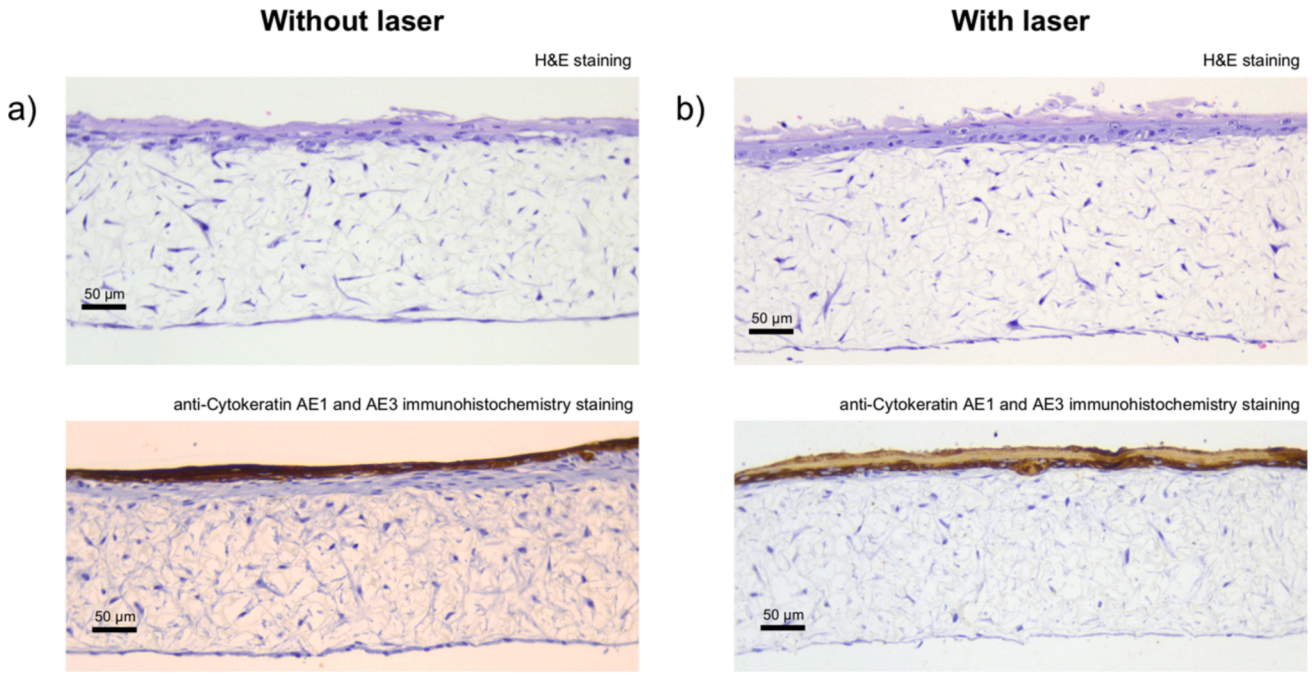

Fig. 12. Representative histopathological images with H&E or anti-Cytokeratin AE1 and AE3 immunohistochemistry staining of *in vitro* 3D reconstructed human skin cross-sections in the absence of laser (a) or 48 h after laser irradiation (b). Scale bars: 50 µm.

20, 25, 30, 35 and 40 s of exposure to the NIR laser irradiation with an irradiance of 0.94 W/cm^2. The histological analysis is shown in Fig. 13.

The animals exposed to 10, 15, 20 and 25 s of irradiation showed no morphological changes. On the contrary, when exposed to irradiation for 30 s or more, all skin samples exhibited multiple lesions, primarily coagulative necrosis affecting the epidermis and, in some cases, the

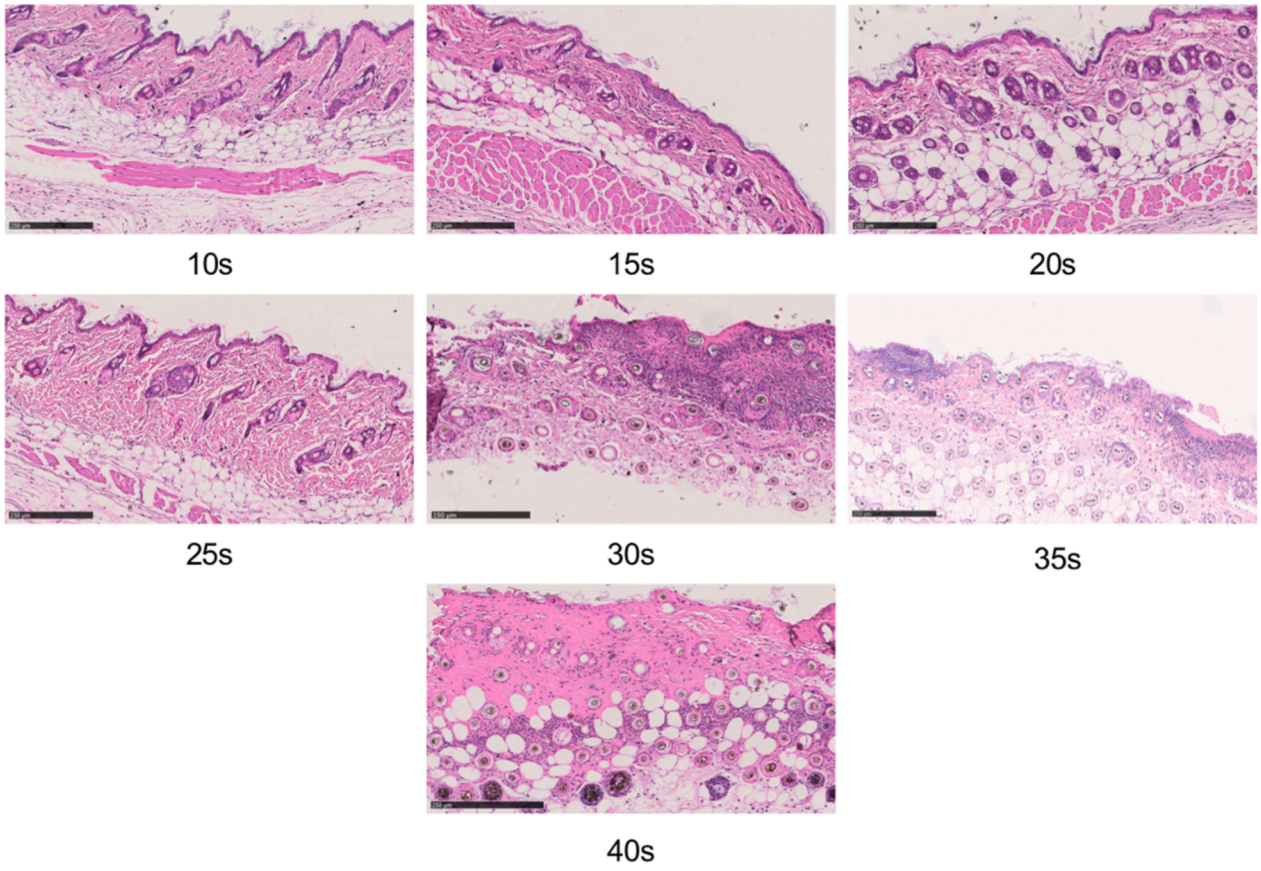

Fig. 13. Histological images (H&E staining) of skin sections irradiated by the NIR laser from various groups of animals subjected to 10, 15, 20, 25, 30, 35 or 40 s of exposure, with a laser irradiance of 0.94 W/cm^2. Each image is representative of the harvested irradiated skin samples. Scale bars represent 250 µm across all images.

dermis. This was accompanied by multifocal areas of dermal inflammatory infiltrates composed mainly of neutrophils. Based on these experiments, 25 s was the exposure time to NIR laser irradiation selected to proceed with the efficacy study.

3.7.2. *Efficacy assessment of PTT using HAOA-AuNPs*

The biological effect of HAOA-AuNPs were evaluated in an *in vivo* murine melanoma model after a single intratumoral administration at a concentration of 3.1 mg/kg of body weight in terms of gold content followed by three NIR laser irradiations of 25 s each (irradiation condition (3)), separated by 48-hours intervals. Tumors were previously induced by subcutaneous injection of B16F10 cells (Fig. 14a). When tumors became visible and palpable, the animals were divided into four groups, including a negative control (induced and no treated), animals exposed to laser irradiation for 25 s, animals that received a single intratumoral administration of HAOA-AuNPs (3.1 mg Au/Kg) without laser irradiation and animals that received a single intratumoral administration of HAOA-AuNPs (3.1 mg Au/Kg) and exposed to three laser irradiation periods of 25 s each separated by 48 h.

The *in vivo* efficacy was evaluated based on the progression of tumor volume recorded on days 0, 2 and 4 for all animals under study. The results are depicted in Fig. 14b.

The combined therapy of HAOA-AuNPs and laser resulted in the greatest impairment of tumor growth. At the end of the protocol, this group of mice presented a mean tumor mass below 350 mm^3, 3- to 5-fold lower compared to control and animals treated with laser or HAOA-AuNPs, respectively.

During the treatment protocol, no adverse behavioral or physical changes were detected and therefore, 24 h after the last irradiation, all animals of each group were sacrificed and organs of interest (liver, kidneys and spleen), blood and tumors were collected.

The tissue index is a parameter commonly used in *in vivo* safety studies, since small changes in organ weight are a sensitive indicator of toxicity, predicting possible morphological changes (Lopes et al., 2023). In this regard, the tissue index values of the liver, kidney and spleen of each group are shown in Table 1.

We observed that the tissue index values of all vital organs analyzed were similar among the different groups, suggesting that no toxicological effects were induced by laser irradiation and intratumoral administration of HAOA-AuNPs alone nor with their combination.

Furthermore, liver enzymes such as aspartate aminotransferase (AST) and alanine aminotransferase (ALT) were measured as they are widely used as biomarkers of tissue damage, in particular, liver toxicity (Kobayashi et al., 2020; Tang et al., 2020). The plasmatic levels of these enzymes for all groups under study are shown in Table 2.

Although a wide range of values in the different groups was observed for AST and ALT, data obtained were within the reference ranges reported by the animal supplier (River, 2024), attesting the preservation of hepatic function.

The safety of the treatment protocol was also supported by

Table 1
Average of tissue index values of the collected organs, namely, liver, kidneys and spleen of each group of C57BL/6 mice at the end of treatment protocol. Control represents the tissue index of animals injected with PBS.

Group of Mice	Tissue Index		
	Liver	Kidney	Spleen
Naïve	22.1 ± 0.6	10.7 ± 0.5	5.0 ± 0.1
Control	21.3 ± 1.3	10.7 ± 0.2	5.1 ± 0.2
Only laser	22.5 ± 0.5	10.5 ± 0.3	6.4 ± 0.5
HAOA-AuNPs	23.9 ± 0.6	10.5 ± 0.3	7.1 ± 0.7
HAOA-AuNPs + laser	22.5 ± 0.3	11.3 ± 0.2	5.9 ± 0.2

Data are presented as mean ± SEM, n ≥ 3.

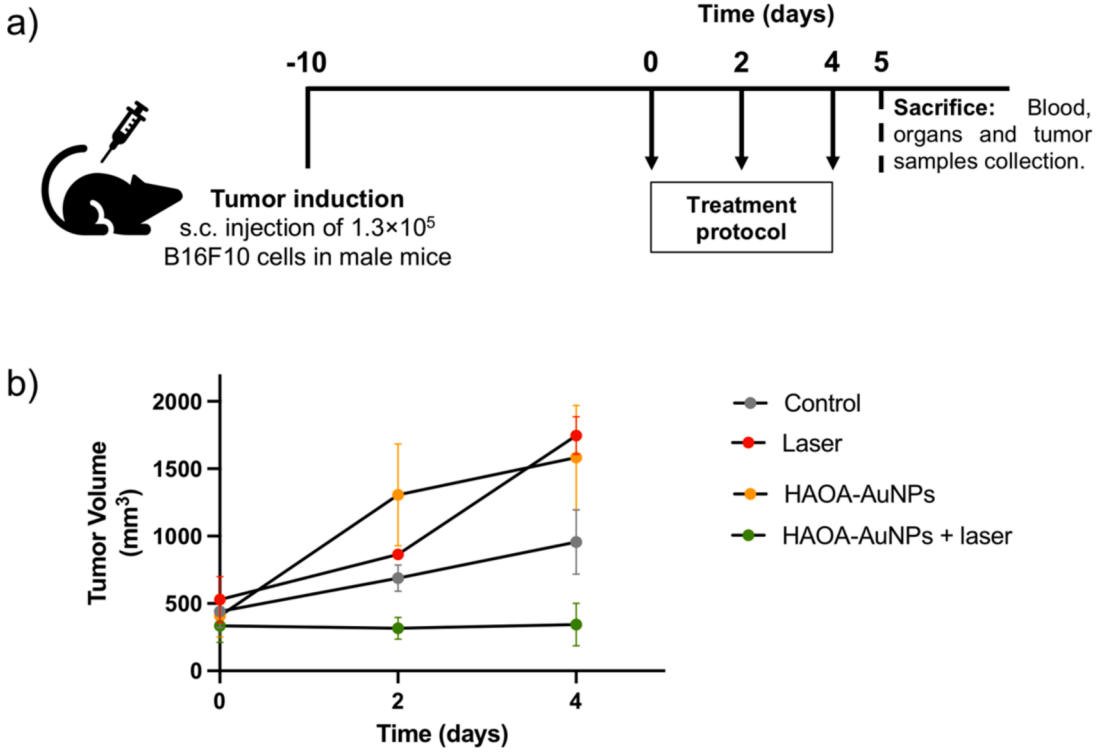

Fig. 14. Efficacy assessment of PTT using HAOA-AuNPs. (a) Experimental protocol for the syngeneic subcutaneous murine melanoma model and (b) average tumor volume (mm^3) of the different groups, namely, animals that received a single intratumoral administration of PBS at day 0 (Control, non-treated), animals exposed to laser irradiation for 25 s at days 0, 2 and 4 (laser), animals that received a single intratumoral administration of HAOA-AuNPs on day 0 (HAOA-AuNPs) and animals that received a single intratumoral administration of HAOA-AuNPs and exposed to laser irradiation for 25 s on days 0 (4 h after injection of HAOA-AuNPs), 2 and 4 (HAOA-AuNPs + laser). Data are presented as mean value ± SEM, n ≥ 3.

Table 2
Plasmatic values of liver enzymes aspartate aminotransferase (AST) and alanine aminotransferase (ALT) of each group of C57BL/6 mice at the end of protocol. Control represents the hepatic transaminases of animals injected with PBS.

Group of Mice	Hepatic transaminases	
	AST	ALT
Naïve	143 ± 9	29 ± 1
Control	295 ± 44	82 ± 25
Only laser	194 ± 56	80 ± 7
HAOA-AuNPs	152 ± 22	66 ± 17
HAOA-AuNPs + laser	253 ± 27	46 ± 6

Data are presented as mean ± SEM, n ≥ 3.

histological analysis, which did not detect morphological changes in any of the organs of the different groups of animals. Representative images are shown in Fig. 15.

On the other hand, and despite favorable physicochemical properties of HAOA-AuNPs for retention and penetration in tumor tissue, particularly the average size above 100 nm and below 400 nm (Haute and Van Berlin, 2017; Deng et al., 2021; Bae and Park, 2011), the possibility of their leakage into the bloodstream could not be discarded, until because increased temperature in the tumor microenvironment resulting from PTT leads to an increased blood flow and capillary vasodilation, including in animal tumors (Wang et al., 2019). Therefore, in parallel, the gold content in the blood, liver, kidneys, spleen and tumor was also determined by ICP-OES 24 h after the last PTT treatment (sacrifice day). The animal groups analyzed were those that received a single intratumoral administration of HAOA-AuNPs on day 0. The results obtained are depicted in Table 3.

According to the results obtained, no traces of gold were analytically detected in the blood, liver, kidneys and spleen of animals. In contrast, and as expected, HAOA-AuNPs were mainly observed in the tumor, with values in the order of 79 and 72 % of the total dose in terms of gold administered for animals that received only HAOA-AuNPs or combined therapy (HAOA-AuNPs with triple laser exposure), respectively.

Table 3
Gold content in terms of percentage of total administered dose in the blood, liver, kidney, spleen and tumor of C57BL/6 mice at the end of protocol.

Group of Mice	Gold content (% of total administered dose)				
	Blood	Liver	Kidney	Spleen	Tumor
HAOA-AuNPs	N.D.	N.D.	N.D.	N.D.	79 ± 3
HAOA-AuNPs + laser	N.D.	N.D.	N.D.	N.D.	72 ± 17

N.D. – not detected; LOD: 0.073 mg/L and LOQ: 0.222 mg/L.

4. Discussion

PTT has emerged as a promising modality in the treatment of cancer, in which cell death occurs through the use of photothermal enhancers capable of converting light energy received by a laser source into thermal energy (Lopes et al., 2022a). Some AuNP formulations combined with PTT, like the AuroLase® system, have already reached clinical safety (Stern et al., 2016) and efficacy (Rastinehad et al., 2019) evaluation stages, specifically in patients with prostate cancer (NCT02680535 and NCT04240639).

Environmental and safety considerations have driven the development and research into the green synthesis of AuNPs for various biomedical applications (Santhosh et al., 2022). Plant extracts, polysaccharides, fungi, algae, bacteria (Ferreira-Gonçalves et al., 2021) but also phytoconstituents such as curcumin (Amini et al., 2024), apigenin (Ngernyuang et al., 2022) and epigallocatechin gallate (Wakayama et al., 2023) as well as rosmarinic acid, used in this study, have been explored as alternatives to the traditionally cytotoxic gold salt reducing agents. In previous studies performed by our group (Lopes et al., 2023), we focused on optimizing and evaluating the *in vitro*, *ex vivo* and *in vivo* safety of a green synthesis method for preparing coated AuNPs. In the present study, our main goal was to evaluate the *in vitro* and *in vivo*

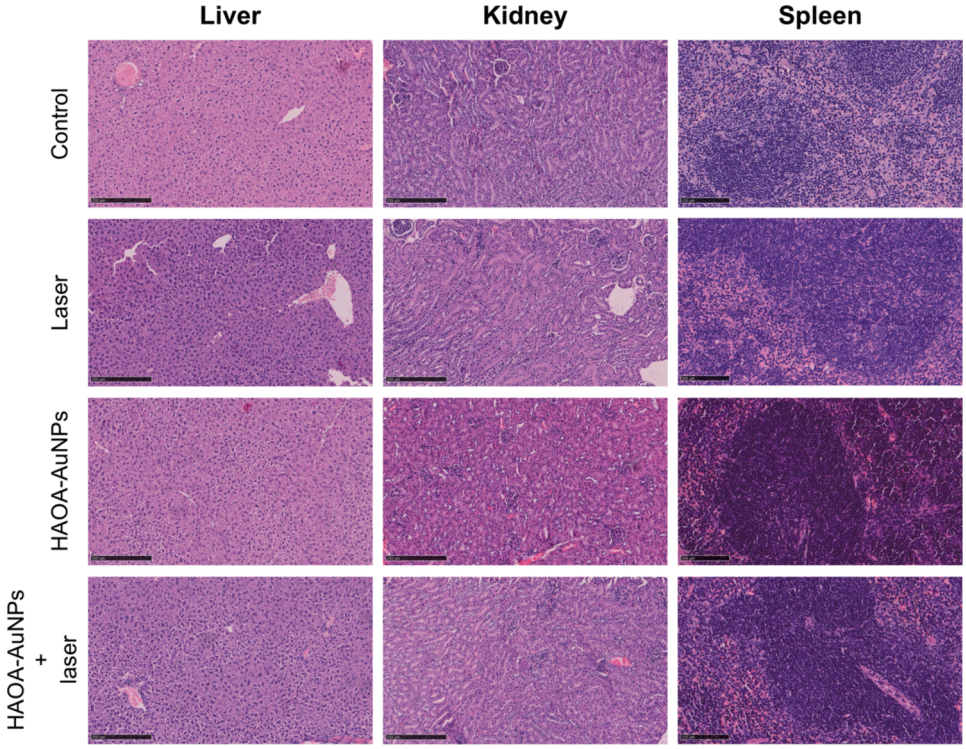

Fig. 15. Histological images (H&E staining) of the liver, kidney and spleen of different groups of animals: control, laser, HAOA-AuNPs, and HAOA-AuNPs + laser. All images are representative of the harvested organs (liver and kidney with 10 × magnification; spleen with 20 × magnification). Scale bars are 250 μm for liver and kidney images and 500 μm for spleen images.

efficacy of the combination of intratumoral administration of HAOA-AuNPs with laser irradiation.

The intratumoral administration route has been increasingly explored, not only for bypassing the bloodstream, thus allowing greater control of its biodistribution, but also by maximizing its accumulation and retention at the tumor site, reducing the incidence of side effects and increasing therapeutic efficacy (Zhao et al., 2021; Yun et al., 2023). Therefore, the intrinsic properties of AuNPs, such as size, PdI, superficial charge, shape or surface chemistry are important factors as they strongly influence the interaction with cells, modulating various aspects such as pharmacokinetics and toxicity (Lopes et al., 2023; Bhattacharjee, 2016; Sabourian et al., 2020; Gong et al., 2015; Adewale et al., 2019; Lin et al., 2015).

Regarding size, the ideal formulation should be small enough to allow uniform diffusion throughout the tumor tissue, but at the same time large enough that, in combination with abnormally disorganized vasculature and poor drainage lymphatic system of the tumor, its extravasation is potentially reduced, thus favoring its retention and consequent internalization by tumor cells (Haute and Van Berlin, 2017; Yun et al., 2023; Miao and Huang, 2015). According to the literature, relatively small nanoparticles (<50 nm) have demonstrated a greater tumor permeation capacity, although they are more easily extravasated from the tumor tissue (Haute and Van Berlin, 2017). Upon extravasation, these small-sized AuNPs have a wide body distribution in healthy organs and tissues such as the thymus, kidney, heart, lung and even brain, in addition to their presence in the liver and spleen (Haute and Van Berlin, 2017; Jong et al., 2008). In contrast, for slightly larger nanoparticles and depending on the type of tumor and/or nanoparticle, it has been described that a maximum size of around 100–200 nm (Haute and Van Berlin, 2017; Deng et al., 2021) and up to 400 nm (Bae and Park, 2011); present a much higher percentage of retention at the tumor site. However, these nanoparticles might present greater difficulty in spreading throughout the tumor.

Therefore, a strategy that seeks the right balance between tumor permeation and retention is imperative. In this regard, the coated AuNP formulation we developed, with a hydrodynamic diameter of about 109 nm fits the above mentioned criteria.

Still concerning size, the homogeneity of the formulation is also important. Although there is no consensus among researchers on acceptable PdI values, as this property depends on the specific nanomaterial considered (Danaei et al., 2018), some authors suggest that nanoparticle samples with a PdI up to 0.3–0.4, which includes the HAOA-AuNPs formulation, are considered adequate (Onugwu et al., 2022; Barhoum et al., 2022; Maguire et al., 2018).

Surface charge of the nanoparticle also influences its *in vivo* behavior (Ferreira-Gonçalves et al., 2022). While positively charged AuNPs are associated with greater toxicity and lower stability, some *in vivo* studies have also suggested a greater accumulation of negatively charged AuNPs at the tumor site (Ferreira-Gonçalves et al., 2022; Honary and Zahir, 2013). When analyzing the surface charge of the AuNPs produced, both formulations presented negative zeta potential values, in line with what was intended.

Furthermore, in optical terms, the coating of the AuNPs formulation resulted in an increase in absorbance at 808 nm, ideal for the intended application and attributed to a cumulative effect of absorption properties of both the AuNPs and the coating, as well as the broadening of the plasmon peak. The intensity and width of the SPR peak is influenced by factors that affect the electronic charge density on the surface of the particles, such as size, shape, structure and composition of the nanoparticles (Huang and El-Sayed, 2010). In this case, the coating applied to the AuNPs not only slightly increased their size but also altered the local dielectric environment. The refractive index of the coating material influences the oscillation of free electrons, modifying the resonance conditions and contributing to the broadening of the plasmon peak (Chanana and Liz-Marzán, 2012). Surface roughness or variations in coating thickness may also play a role in this effect (Rodríguez-Fernández et al., 2009). In this context, the use of NIR light in this type of therapy is important, as it minimizes light absorption by biological tissues, thereby increasing the penetration depth (Lopes et al., 2023; Ferreira-Gonçalves et al., 2022; Souza-Barros et al., 2018).

Besides the coating material, particle morphology will influence not only the *in vivo* behavior of AuNPs, but also its optical properties (Ferreira-Gonçalves et al., 2022). The morphology of uncoated and HAOA-AuNPs did not vary significantly except for the notable coating layer observed for the HAOA-AuNPs. Three different populations were observed. The symmetry and large contact area of spherical nanoparticles allow for quicker and more uniform internalization (Petros and DeSimone, 2010). However asymmetric structures with sharper tips, corners and edges enhance plasmonic heating, favoring the photothermal conversion efficiency (Cui et al., 2023). The observed diversity of shapes, which also supports the PdI values obtained, has been consistent across all batches produced and is associated with green synthetic methods (Ferreira-Gonçalves et al., 2022), as is the case of this preparation method. In fact, this is even a positive characteristic with regard to the optical properties of the formulation. As described in literature, the mixture of plasmonic nanoparticles of different sizes and shapes allows the absorption spectrum to be broadened (Cui et al., 2023; Ortiz-Castillo et al., 2020).

Preclinical studies involving cell cultures and animal models are crucial for evaluating the safety and efficacy of this combined therapy. In this context, in the absence of laser irradiation and as observed in a previous work (Lopes et al., 2023), both formulations proved to be safe in both melanoma cell lines. A single reduction in cell viability was only observed for murine B16F10 cells but at the highest concentration tested (400 μM). In all other cases, in the presence of uncoated and HAOA-AuNPs, cell viability always remained above 70 %, which according to ISO10993-5:2009(E) attests its safety (International Organization for Standardization. Biological evaluation of medical devices-Part 5: Tests for in vitro cytotoxicity. ISO, 2009). In turn, laser irradiation itself has also been shown to be safe for both cell lines.

In terms of *in vitro* efficacy, the combination of uncoated and HAOA-AuNPs in different concentrations with laser irradiation in murine B16F10 and human A375 melanoma cell lines resulted in a great loss of cell viability. The B16F10 cells exhibited high sensitivity to PTT, with an approximately 80 % reduction in cell viability at the lowest concentration tested (100 μM). In this cell line, increasing AuNP concentrations did not further reduce cell viability beyond the level observed at the lowest concentration. In contrast, the human A375 cell line required an AuNP concentration of 400 μM to achieve a comparable effect to that observed in the murine cell line. As previously noted, the photothermal effect is a complex process that can be influenced by several aspects, including the shape and size of the AuNPs, their SPR with incident light, their absorbance and scattering properties, concentration, irradiation dose, but particularly by the formation of a protein corona around the AuNPs when incubated within the cells (Nandakumar et al., 2021), the distribution of the AuNPs within cells (Villuendas et al., 2022) and the type of cell line (Amaral et al., 2024). Previous studies have shown that cell viability outcomes can vary across cell lines like HaCat, HCT-116, A375, and MCF-7, even under identical experimental conditions (using the same AuNP formulation and irradiation dose) (Amaral et al., 2024). This variability reflects inherent biological differences and distinct sensitivities among cell lines.

On the other hand, cell interaction is also an important property for any nanomaterial. AuNPs can be functionalized with targeting molecules (e.g., antibodies, sugars, ligands of cell receptors) that specifically bind to melanoma cells. The selection of HA was based on the described features of this polymer. This ensures selective accumulation of AuNPs in the tumor tissue. HA is a biocompatible, biodegradable and low immunogenicity polysaccharide that targets AuNPs to cancer cells which overexpress CD44 receptors (Cirillo, 2023; Kesharwani et al., 2022). Thus, this linking would allow an improvement of the formulation in the target area through the affinity of HA for its receptor (Cirillo,

2023). In this case, the ability of uncoated and HAOA-AuNPs to be internalized by melanoma cells was evaluated after a period of 4 h of incubation and at a concentration of 200 μM. However, and contrary to expectations, the *in vitro* results showed that for each melanoma cell line tested, the percentage of internalization was similar for uncoated and HAOA-AuNPs, with a mean value of around 42 and 51 % in the B16F10 and A375 cell lines, respectively.

Notably, previously published studies from our group (Lopes et al., 2020; Ferreira-Gonçalves et al., 2024), demonstrated that even under laser irradiation, the formulated AuNPs exhibited low toxicity and high biocompatibility in healthy keratinocyte cell lines (HaCat), further supporting their selectivity for tumor cells over healthy skin cells. Furthermore and in this context, some authors have reported a protective effect of hyaluronic acid over radiation exposure-induced keratinocytes damage (Sörgel et al., 2022; Hašová et al., 2011). Therefore, and based on their abovementioned better physicochemical and optical properties, at this point, HAOA-AuNPs at 200 μM were selected to proceed to the evaluation of associated cell death mechanisms of combined therapy through cell cycle and Annexin V/PI as well as for *in vivo* efficacy assessment. Thermal activation study of HAOA-AuNPs was carried out after their irradiation on a phantom model and the results are presented in Supplementary Material (Figure S3).

With regard to the mechanism of action associated with PTT on the cell cycle, while HAOA-AuNPs and laser irradiation alone did not interfere, the combined therapy (HAOA-AuNPs and laser) promoted a significant cell arrest in S phase in both B16F10 and A375 cell lines, 24 h after laser irradiation. A similar effect was also observed by other authors after photothermal exposure of polydopamine-coated branched Au-Ag nanoparticles in human bladder cancer cells (Zhao et al., 2018). During the cell cycle there are several checkpoints that allow cells to repair possible DNA damage, however, their deregulation before DNA repair can lead to the activation of apoptotic cascade and consequent cell death (Li et al., 2019). Cell death in PTT is based on increased temperature and is normally divided into two types: apoptosis and necrosis (Kim et al., 2023). Annexin V and PI are frequently combined to detect differences in cell plasma membrane permeability, thus distinguishing viable, apoptotic and necrotic cells (Kus-Liskiewicz et al., 2021; Worsley et al., 2022). Our results showed that the application of the combined therapy of HAOA-AuNPs and laser irradiation caused a significant increase in the percentage of cells in late apoptosis compared to the control group and the groups subjected to HAOA-AuNPs or laser irradiation. It is described that during the late stage of apoptosis, there is membrane blebbing, ultrastructural modification of some cytoplasmic organelles and even loss of integrity of the plasma membrane (Wong, 2011), with the latter being the reason why there is cells positively stained for Annexin V and PI. Apoptotic cells are normally phagocytosed before the formation of apoptotic bodies, which does not happen in an artificial cell culture environment, leading to degradation that resembles necrosis and which is called secondary necrosis (Wong, 2011; Ziegler and Groscurth, 2004).

Overall, the results regarding the elucidation of the mechanism of action indicate that the combined therapy reduced cell proliferation, inducing apoptosis and a cell cycle arrest at S-phase in both B16F10 and A375 cell lines. Furthermore, the *in vitro* 3D human skin model also confirmed the safety of the laser at the tested dose as observed for 2D cell models performed.

Finally, considering the therapeutic potential shown *in vitro* for the murine and human melanoma cell lines tested, an *in vivo* syngeneic melanoma model was performed through subcutaneous implantation of B16F10 cells. A preliminary *in vivo* safety assay in healthy C57BL/6 mice demonstrated that exposure to laser could not be longer than 25 s. Therefore, 25 s of irradiation, with an irradiance of 0.94 W/cm^2 and corresponding to a dose of 24 J/cm^2, were selected. It should be noted that C57BL/6 mice have black fur, absorbing a greater amount of energy on the skin surface and not allowing radiation to reach deeper areas being more susceptible to skin burns (Stadler et al., 2004; Setchfield et al., 2024). In previous published work of our group, immune-deficient hairless mice were subjected to an irradiance of 2.5 W/cm^2 during 5 and 10 min without signals of skin damage (Lopes et al., 2021).

With the laser safe dose adjusted, the efficacy of intratumoral administration of HAOA-AuNPs in combination with laser irradiation was carried out in a subcutaneous C57BL/6 melanoma model. It was observed that the combined therapy resulted in a superior impairment of tumor growth progression compared to control and animals treated with HAOA-AuNPs or laser alone. These last two groups even had enhanced tumor progression compared to the control group. Using the same *in vivo* model and similar dose of NIR irradiation as the one tested in our work, de Souza Contatori and co-workers reported an increase in the invasiveness of pigmented melanoma cells (Contatori et al., 2022). In the case of the group of animals that received only the coated AuNPs formulation, in the absence of photothermal treatment, this phenomena may contribute to proliferation mediated by the CD44 receptor-hyaluronic acid interactions (Assmann et al., 2001).

Data regarding plasmatic levels of liver enzymes AST and ALT as well as tissue index and histological analysis of the different organs collected showed no significant differences among all tested animals either in healthy or in subcutaneous melanoma mice independent of the treatment protocol, thus demonstrating the safety of PTT. Furthermore, evaluation of the gold concentration in blood, liver, kidneys, spleen and tumors showed that a very high percentage of the HAOA-AuNPs administered was retained in the tumor until the end of the experimental protocol, with no gold concentration being detected in the blood or in any of the evaluated metabolic and elimination organs. Computed tomography studies performed by us, using AuNPs with similar characteristics, have also shown that even one month after subcutaneous administration, in the right flank of healthy animals, the particles continued to be retained (Ferreira-Gonçalves et al., 2024).

5. Conclusions

The high morbidity and mortality rates associated with melanoma have been imposing continuous research of new and better therapeutic options. In this study, PTT using AuNPs as photothermal enhancers was evaluated for *in vitro* and *in vivo* efficacy against melanoma. Uncoated and HAOA-AuNPs demonstrated a high cellular internalization rate in B16F10 and A375 melanoma cell lines. The combined therapy of AuNPs (whether coated or not) and laser exhibited a pronounced reduction in viability compared to AuNPs or laser alone. This dual therapy induced S-phase cell cycle arrest and late apoptosis in both cell lines. Preliminary studies in a murine syngeneic subcutaneous melanoma model demonstrated that HAOA-AuNPs were strongly accumulated at the tumor site and when combined with laser irradiation resulted in a significant impairment of tumor progression.

These promising results suggest that combination of AuNPs and NIR-laser irradiation is safe and holds therapeutic potential in the treatment of superficial and localized melanoma.

CRediT authorship contribution statement

Joana Lopes: Writing – original draft, Methodology, Investigation, Formal analysis. **Carla M. Rodrigues:** Writing – review & editing, Methodology, Investigation, Formal analysis. **Ana Godinho-Santos:** Writing – review & editing, Methodology, Investigation, Formal analysis. **João M.P. Coelho:** Writing – review & editing, Methodology, Investigation, Formal analysis, Conceptualization. **Luís C. Cabaço:** Writing – review & editing, Methodology, Investigation, Formal analysis. **Duarte C. Barral:** Writing – review & editing, Methodology, Investigation, Formal analysis. **Pedro Faísca:** Writing – review & editing, Methodology, Investigation, Formal analysis. **José Catarino:** Writing – review & editing, Methodology, Investigation, Formal analysis. **Daniela Nunes:** Writing – review & editing, Methodology, Investigation, Formal analysis. **Elvira Fortunato:** Writing – review & editing,

Investigation. **Rodrigo Martins:** Writing – review & editing, Investigation. **Cecília M.P. Rodrigues:** Writing – review & editing, Supervision, Methodology, Investigation, Formal analysis. **Maria Manuela Gaspar:** Writing – review & editing, Supervision, Methodology, Investigation, Funding acquisition, Formal analysis, Conceptualization. **Catarina Pinto Reis:** Writing – review & editing, Supervision, Methodology, Investigation, Funding acquisition, Formal analysis, Conceptualization.

Funding

The authors acknowledge Fundação para a Ciência e a Tecnologia (FCT) for the essential financial support under the project's references UIDB/00645/2020 (https://doi.org/10.54499/UIDB/00645/2020), UIDP/00645/2020 (https://doi.org/10.54499/UIDP/00645/2020), UIDB/04138/2020, UIDP/04138/2020, PTDC/MED-QUI/31721/2017 and PTDC/QUI-QIN/0586/2020 as well as for the PhD fellowship SFRH/BD/148044/2019.

Declaration of competing interest

The authors declare that they have no known competing financial interests or personal relationships that could have appeared to influence the work reported in this paper.

Acknowledgments

The authors would like to thank to Professor Rute Noiva from the Faculty of Veterinary Medicine, Universidade de Lisboa, for her valuable assistance on histological analysis and Rita Bassolino for her support in samples preparation to perform the Annexin V/PI assay.

Appendix A. Supplementary data

Supplementary Materials: The following supporting information can be found in Supplementary Materials. Figure S1. Stability of HAOA-AuNPs in water after 1 month of storage at 4 °C and room temperature, as well as on the day of preparation in PBS. Data are presented as mean ± SD, n ≥ 3. Figure S3. Evaluation of thermal activity of HAOA-AuNPs at a concentration of 200 μM under NIR laser irradiation over 10 min. Data are presented as mean value ± SD, n = 3. Figure S2. Gating strategy for apoptosis analysis by flow cytometry. Debris were excluded before assessing propidium iodide (PI) and Annexin V fluorescence, by selecting first double negative (DN) fraction, that drawing a gate to select Debris, and then creating a Not-Debris gate to assess early apoptotic, late apoptotic, necrotic and live cell populations.Supplementary data to this article can be found online at https://doi.org/10.1016/j.ijpharm.2024.124952.

Data availability

Data will be made available on request.

References

Adewale, O.B., Davids, H., Cairncross, L., Roux, S., 2019. Toxicological behavior of gold nanoparticles on various models: influence of physicochemical properties and other factors. *Int. J. Toxicol.* 38, 357–384.

Amaral, M.N., Nunes, D., Fortunato, E., Martins, R., Rodrigues, C., Faísca, P., Ferreira, H. A., Coelho, J.M.P., Gaspar, M.M., Reis, C.P., 2024. Gold nanoparticles for photothermal therapy – Influence of experimental conditions on the properties of resulting AuNPs. *J. Drug Deliv. Sci. Technol.* 101, 106215.

Amini, S.M., Emami, T., Rashidi, M., Zarrinnahad, H., 2024. Curcumin-gold nanoformulation: Synthesis, characterizations and biomedical application. *Food Biosci.* 57, 103446.

Arem, H., Loftfield, E., 2018. Cancer Epidemiology: A Survey of Modifiable Risk Factors for Prevention and Survivorship. *Am. J. Lifestyle Med.* 12, 200–210.

Assmann, V., Fieber, C., Herrlich, P., Hofmann, M., Termeer, C.C., Ahrens, T., Simon, J. C., 2001. CD44 is the Principal Mediator of Hyaluronic-Acid-Induced Melanoma Cell Proliferation. *J. Invest. Dermatol.* 116, 93–101.

Bae, Y.H., Park, K., 2011. Targeted drug delivery to tumors: myths, reality and possibility. *J. Control. Release* 153, 198–205.

Barhoum, A., García-Betancourt, M.L., Jeevanandam, J., Hussien, E.A.; Mekkawy, S.A., Mostafa, M., Omran, M.M., S. Abdalla, M., Bechelany, M., 2022. Review on Natural, Incidental, Bioinspired, and Engineered Nanomaterials: History, Definitions, Classifications, Synthesis, Properties, Market, Toxicities, Risks, and Regulations. Nanomaterials, *12*, 177.

Bhattacharjee, S., 2016. DLS and zeta potential – What they are and what they are not? *J. Control. Release* 235, 337–351.

Biemar, F., Foti, M., 2013. Global progress against cancer—challenges and opportunities. *Cancer Biol. Med.* 10, 183–186.

Chanana, M., Liz-Marzán, L.M., 2012. Coating matters: the influence of coating materials on the optical properties of gold nanoparticles. *Nanophotonics* 1, 199–220.

Cirillo, N., 2023. The Hyaluronan/CD44 Axis: A Double-Edged Sword in Cancer. *Int. J. Mol. Sci.* 24, 15812.

Contatori, C.G. de S., Silva, C.R., Pereira, S. de T., Rodrigues, M.F.S.D., Luna, A.C. de L., Marques, M.M., Ribeiro, M.S., 2022. Responses of melanoma cells to photobiomodulation depend on cell pigmentation and light parameters. J. Photochem. Photobiol. B Biol. 235, 112567.

Cui, X., Ruan, Q., Zhuo, X., Xia, X., Hu, J., Fu, R., Li, Y., Wang, J., Xu, H., 2023. Photothermal Nanomaterials: A Powerful Light-to-Heat Converter. *Chem. Rev.* 123, 6891–6952.

Danaei, M., Dehghankhold, M., Ataei, S., Hasanzadeh Davarani, F., Javanmard, R., Dokhani, A., Khorasani, S., Mozafari, M.R., 2018. Impact of particle size and polydispersity index on the clinical applications of lipidic nanocarrier systems. *Pharmaceutics* 10, 57.

Deng, M., Rao, J.-D., Guo, R., Li, M., He, Q., 2021. Size-adjustable nano-drug delivery systems for enhanced tumor retention and penetration. *Pharm. Front.* 03, e98–e112.

Ernst, M., Giubellino, A., 2022. The Current State of Treatment and Future Directions in Cutaneous Malignant Melanoma. *Biomedicines* 10, 822.

Ferreira-Gonçalves, T., Ferreira, D., Ferreira, H.A., Reis, C.P., 2021. Nanogold-based materials in medicine: from their origins to their future. *Nanomedicine* 16, 2695–2723.

Ferreira-Gonçalves, T., Gaspar, M.M., Coelho, J.M.P., Marques, V., Viana, A.S., Ascensão, L., Carvalho, L., Rodrigues, C.M.P., Ferreira, H.A., Ferreira, D., et al., 2022. The Role of Rosmarinic Acid on the Bioproduction of Gold Nanoparticles as Part of a Photothermal Approach for Breast Cancer Treatment. *Biomolecules* 12, 71.

Ferreira-Gonçalves, T., Nunes, D., Fortunato, E., Martins, R., de Almeida, A.P., Carvalho, L., Ferreira, D., Catarino, J., Faísca, P., Ferreira, H.A., et al., 2024. Rational approach to design gold nanoparticles for photothermal therapy: the effect of gold salt on physicochemical, optical and biological properties. *Int. J. Pharm.* 650, 123659.

Golemis, E.A., Scheet, P., Beck, T.N., Scolnick, E.M., Hunter, D.J., Hawk, E., Hopkins, N., 2018. Molecular mechanisms of the preventable causes of cancer in the United States. *Genes Dev.* 32, 868–902.

Gong, N., Chen, S., Jin, S., Zhang, J., Wang, P.C., Liang, X.-J., 2015. Effects of the physicochemical properties of gold nanostructures on cellular internalization. *Regen. Biomater.* 2, 273–280.

Hall, M.J., Lopes-Ventura, S., Neto, M.V., Charneca, J., Zoio, P., Seabra, M.C., Oliva, A., Barral, D.C., 2022. Reconstructed human pigmented skin/epidermis models achieve epidermal pigmentation through melanocore transfer. *Pigment Cell Melanoma Res.* 35, 425–435.

Han, H.S., Choi, K.Y., 2021. Advances in Nanomaterial-Mediated Photothermal Cancer Therapies: Toward Clinical Applications. *Biomedicines* 9, 305.

Hannon, G., Tansi, F.L., Hilger, I., Prina-Mello, A., 2021. The Effects of Localized Heat on the Hallmarks of Cancer. *Adv. Ther.* 4.

Hašová, M., Crhák, T., Šafránková, B., Dvořáková, J., Muthný, T., Velebný, V., Kubala, L., 2011. Hyaluronan minimizes effects of UV irradiation on human keratinocytes. *Arch. Dermatol. Res.* 303, 277–284.

Haute, D., Van Berlin, J.M., 2017. challenges in realizing selectivity for nanoparticle biodistribution and clearance: lessons from gold nanoparticles. *Ther. Deliv.* 8, 763–774.

Hipólito, A., Xavier, R., Brito, C., Tomás, A., Lemos, I., Cabaço, L.C., Silva, F., Oliva, A., Barral, D.C., Vicente, J.B., et al., 2024. BRD9 status is a major contributor for cysteine metabolic remodeling through MST and EAAT3 modulation in malignant melanoma. *Biochim. Biophys. Acta - Mol. Basis Dis.* 1870, 166983.

Honary, S., Zahir, F., 2013. Effect of zeta potential on the properties of nano-drug delivery systems - a review (part 2). *Trop. J. Pharm. Res.* 12, 265–273.

Huang, X., El-Sayed, M.A., 2010. Gold nanoparticles: Optical properties and implementations in cancer diagnosis and photothermal therapy. *J. Adv. Res.* 1, 13–28.

Imashiro, C., Takeshita, H., Morikura, T., Miyata, S., Takemura, K., Komotori, J., 2021. Development of accurate temperature regulation culture system with metallic culture vessel demonstrates different thermal cytotoxicity in cancer and normal cells. *Sci. Rep.* 11, 21466.

International Agency for Research on Cancer, Cancer Tomorrow - Estimated number of deaths for all cancers from 2022 to 2025 Available online: https://gco.iarc.fr/tomorrow/en/dataviz/isotype?years=2025&single_unit=500000&types=1 (accessed on July 30, 2024).

International Agency for Research on Cancer, Cancer Tomorrow - Estimated number of new cases of all cancers from 2022 to 2025 Available online: https://gco.iarc.fr/tomorrow/en/dataviz/isotype?years=2025&single_unit=500000&types=0 (accessed on July 30, 2024).

International Organization for Standardization. *Biological evaluation of medical devices- Part 5: Tests for in vitro cytotoxicity. ISO 10993-5:2009*.
Jin, H., Xie, X., Hu, B., Gao, F., Zhou, J., Zhang, Y., Du, L., Wang, X., Zhao, L., Zhang, X., et al., 2013. Hyperthermia inhibits the proliferation and invasive ability of mouse malignant melanoma through TGF-β1. *Oncol. Rep.* 29, 725–734.
Kaub, L., Schmitz, C., 2022. More than Ninety Percent of the Light Energy Emitted by Near-Infrared Laser Therapy Devices Used to Treat Musculoskeletal Disorders Is Absorbed within the First Ten Millimeters of Biological Tissue. *Biomedicines* 10, 3204.
Kesharwani, P., Chadar, R., Sheikh, A., Rizg, W.Y., Safhi, A.Y., 2022. CD44-Targeted Nanocarrier for Cancer Therapy. *Front. Pharmacol.* 12.
Kim, D., Paik, J., Kim, H., 2023. Effect of gold nanoparticles distribution radius on photothermal therapy efficacy. *Sci. Rep.* 13, 12135.
Kobayashi, A., Suzuki, Y., Sugai, S., 2020. Specificity of transaminase activities in the prediction of drug-induced hepatotoxicity. *J. Toxicol. Sci.* 45, 515–537.
Kus-Liskiewicz, M., Fickers, P., Ben Tahar, I., 2021. Biocompatibility and Cytotoxicity of Gold Nanoparticles: Recent Advances in Methodologies and Regulations. Int. J. Mol. Sci. 22, 10952.
Li, L., Han, X., Wang, M., Li, C., Jia, T., Zhao, X., 2021. Recent advances in the development of near-infrared organic photothermal agents. *Chem. Eng. J.* 417, 128844.
Li, Y., Pan, J., Gou, M., 2019. The Anti-Proliferation, Cycle Arrest and Apoptotic Inducing Activity of Peperomin E on Prostate Cancer PC-3 Cell Line. *Molecules* 24, 1472.
Lin, Z., Monteiro-Riviere, N.A., Riviere, J.E., 2015. Pharmacokinetics of metallic nanoparticles. *Wires Nanomed. Nanobiotechnol.* 7, 189–217.
Lin, A.Y., Yang, E., Rink, J.S., Xu, D., Miller, S., Gordon, L.I., 2023. Photoablation with the Aurolase System Reduces T Cell Exhaustion and Synergizes with Immunotherapies in Lymphoma. *Blood* 142, 2825.
Logghe, T., Zwol, E. van, Immordino, B., Cruys, K. Van den, Peeters, M., Giovannetti, E., Bogers, J., 2024. Hyperthermia in Combination with Emerging Targeted and Immunotherapies as a New Approach in Cancer Treatment. Cancers (Basel). 16, 505.
Jong, W.H. De, Hagens, W.I., Krystek, P., Burger, M.C., Sips, A.J.A.M., Geertsma, R.E., 2008. Particle size-dependent organ distribution of gold nanoparticles after intravenous administration. Biomaterials 29, 1912–1919.
Lopes, J., Coelho, J.M.P., Vieira, P.M.C., Viana, A.S., Gaspar, M.M., Reis, C., 2020. Preliminary Assays towards Melanoma Cells Using Phototherapy with Gold-Based Nanomaterials. Nanomater. 10, 1536.
Lopes, J., Ferreira-Gonçalves, T., Figueiredo, I.V., Rodrigues, C.M.P., Ferreira, H., Ferreira, D., Viana, A.S., Faísca, P., Gaspar, M.M., Coelho, J.M.P., et al., 2021. Proof-of-Concept Study of Multifunctional Hybrid Nanoparticle System Combined with NIR Laser Irradiation for the Treatment of Melanoma. *Biomolecules* 11, 511.
Lopes, J., Rodrigues, C.M.P., Gaspar, M.M., Reis, C.P., 2022a. How to Treat Melanoma? The Current Status of Innovative Nanotechnological Strategies and the Role of Minimally Invasive Approaches like PTT and PDT. Pharmaceutics 14, 1817.
Lopes, J., Ferreira-Gonçalves, T., Ascensão, L., Viana, A.S., Carvalho, L., Catarino, J., Faísca, P., Oliva, A., de Barros, D.P.C., Rodrigues, C.M.P., et al., 2023. Safety of Gold Nanoparticles: From In Vitro to In Vivo Testing Array Checklist. *Pharmaceutics* 15, 1120.
Lopes, J., Rodrigues, C.M.P., Gaspar, M.M., Reis, C.P., 2022b. Melanoma Management: From Epidemiology to Treatment and Latest Advances. Cancers (basel). 14, 4652.
Maguire, C.M., Rösslein, M., Wick, P., Prina-Mello, A., 2018. Characterisation of particles in solution – a perspective on light scattering and comparative technologies. *Sci. Technol. Adv. Mater.* 19, 732–745.
Martins, A., Ferreira, B.C., Gaspar, M.M., Vieira, S., Lopes, J., Viana, A.S., Paulo, A., Mendes, F., Campello, M.P.C., Martins, R., et al., 2024. Enhanced Cytotoxicity against a Pancreatic Cancer Cell Line Combining Radiation and Gold Nanoparticles. *Pharmaceutics* 16, 900.
Matos, C.P., Albino, M., Lopes, J., Viana, A.S., Côrte-Real, L., Mendes, F., Pessoa, J.C., Tomaz, A.I., Reis, C.P., Gaspar, M.M., et al., 2022. New iron(III) anti-cancer aminobisphenolate/phenanthroline complexes: Enhancing their therapeutic potential using nanoliposomes. *Int. J. Pharm.* 623, 121925.
Miao, L., Huang, L., 2015. Exploring the Tumor Microenvironment with Nanoparticles. In: Nanotechnology-Based Precision Tools for the Detection and Treatment of Cancer. Springer, Cham, pp. 193–226.
Naik, P.P., 2021. Cutaneous Malignant Melanoma: A Review of Early Diagnosis and Management. *World J. Oncol.* 12, 7–19.
Nandakumar, A., Wei, W., Siddiqui, G., Tang, H., Li, Y., Kakinen, A., Wan, X., Koppel, K., Lin, S., Davis, T.P., et al., 2021. Dynamic Protein Corona of Gold Nanoparticles with an Evolving Morphology. *ACS Appl. Mater. Interfaces* 13, 58238–58251.
Ngernyuang, N., Wongwattanakul, M., Charusirisawad, W., Shao, R., Limpaiboon, T., 2022. Green synthesized apigenin conjugated gold nanoparticles inhibit cholangiocarcinoma cell activity and endothelial cell angiogenesis in vitro. *Heliyon* 8, e12028.
Onugwu, A.L., Attama, A.A., Nnamani, P.O., Onugwu, S.O., Onuigbo, E.B., Khutoryanskiy, V.V., 2022. Development and optimization of solid lipid nanoparticles coated with chitosan and poly(2-ethyl-2-oxazoline) for ocular drug delivery of ciprofloxacin. *J. Drug Deliv. Sci. Technol.* 74, 103527.
Ortiz-Castillo, J.E., Gallo-Villanueva, R.C., Madou, M.J., Perez-Gonzalez, V.H., 2020. Anisotropic gold nanoparticles: A survey of recent synthetic methodologies. *Coord. Chem. Rev.* 425, 213489.
Patel, M., Eckburg, A., Gantiwala, S., Hart, Z., Dein, J., Lam, K., Puri, N., 2021. Resistance to Molecularly Targeted Therapies in Melanoma. *Cancers (basel)*. 13, 1115.
Petros, R.A., DeSimone, J.M., 2010. Strategies in the design of nanoparticles for therapeutic applications. *Nat. Rev. Drug Discov.* 9, 615–627.
Piccolo, O., Lincoln, J.D., Melong, N., Orr, B.C., Fernandez, N.R., Borsavage, J., Berman, J.N., Robar, J., Ha, M.N., 2022. Radiation dose enhancement using gold nanoparticles with a diamond linear accelerator target: a multiple cell type analysis. *Sci. Rep.* 12, 1559.
Piña-Sánchez, P., Chávez-González, A., Ruiz-Tachiquín, M., Vadillo, E., Monroy-García, A., Montesinos, J.J., Grajales, R., Barrera, M.G. de la, Mayani, H., 2021. Cancer Biology, Epidemiology, and Treatment in the 21st Century: Current Status and Future Challenges From a Biomedical Perspective. Cancer Control 28, 1–21.
Pinho, J.O., Matias, M., Godinho-Santos, A., Amaral, J.D., Mendes, E., Perry, M.J., Francisco, A.P., Rodrigues, C.M.P., Gaspar, M.M., 2023. A step forward on the in vitro and in vivo assessment of a novel nanomedicine against melanoma. *Int. J. Pharm.* 640, 123011.
Pinho, J.O., Matias, M., Marques, V., Eleutério, C., Fernandes, C., Gano, L., Amaral, J.D., Mendes, E., Perry, M.J., Moreira, J.N., et al., 2023. Preclinical validation of a new hybrid molecule loaded in liposomes for melanoma management. *Biomed. Pharmacother.* 157, 114021.
Rastinehad, A.R., Anastos, H., Wajswol, E., Winoker, J.S., Sfakianos, J.P., Doppalapudi, S.K., Carrick, M.R., Knauer, C.J., Taouli, B., Lewis, S.C., et al., 2019. Gold nanoshell-localized photothermal ablation of prostate tumors in a clinical pilot device study. *Proc. Natl. Acad. Sci.* 116, 18590–18596.
River, C. C57BL/6 Mice Datasheet | Charles River Available online: https://www.criver.com/products-services/find-model/c57bl6-mouse?region=3616 (accessed on May 23, 2024).
Rodríguez-Fernández, J., Funston, A.M., Pérez-Juste, J., Álvarez-Puebla, R.A., Liz-Marzán, L.M., Mulvaney, P., 2009. The effect of surface roughness on the plasmonic response of individual sub-micron gold spheres. *Phys. Chem. Chem. Phys.* 11, 5909.
Sabourian, P., Yazdani, G., Ashraf, S.S., Frounchi, M., Mashayekhan, S., Kiani, S., Kakkar, A., 2020. Effect of physico-chemical properties of nanoparticles on their intracellular uptake. *Int. J. Mol. Sci.* 21, 8019.
Santhosh, P.B., Genova, J., Chamati, H., 2022. Green Synthesis of Gold Nanoparticles: An Eco-Friendly Approach. *Chemistry (easton)*. 4, 345–369.
Schuemann, J., Berbeco, R., Chithrani, D.B., Cho, S.H., Kumar, R., McMahon, S.J., Sridhar, S., Krishnan, S., 2016. Roadmap to Clinical Use of Gold Nanoparticles for Radiation Sensitization. *Int. J. Radiat. Oncol.* 94, 189–205.
Setchfield, K., Gorman, A., Simpson, A.H.R.W., Somekh, M.G., Wright, A.J., 2024. Effect of skin color on optical properties and the implications for medical optical technologies: a review. *J. Biomed. Opt.* 29, 010901.
Shanei, A., Akbari-Zadeh, H., 2019. Investigating the Sonodynamic-Radiosensitivity Effect of Gold Nanoparticles on HeLa Cervical Cancer Cells. *J. Korean Med. Sci.* 34.
Silva, C.O., Rijo, P., Molpeceres, J., Ascensão, L., Roberto, A., Fernandes, A.S., Gomes, R., Pinto Coelho, J.M., Gabriel, A., Vieira, P., et al., 2016. Bioproduction of Gold Nanoparticles for Photothermal Therapy. *Ther. Deliv.* 7, 287–304.
Sörgel, C.A., Schmid, R., Stadelmann, N., Weisbach, V., Distel, L., Horch, R.E., Kengelbach-Weigand, A., 2022. IGF-I and Hyaluronic Acid Mitigate the Negative Effect of Irradiation on Human Skin Keratinocytes. *Cancers (basel)*. 14, 588.
Souza-Barros, L., Dhaidan, G., Maunula, M., Solomon, V., Gabison, S., Lilge, L., Nussbaum, E.L., 2018. Skin color and tissue thickness effects on transmittance, reflectance, and skin temperature when using 635 and 808 nm lasers in low intensity therapeutics. *Lasers Surg. Med.* 50, 291–301.
Stadler, I., Lanzafame, R.J., Oskoui, P., Zhang, R.-Y., Coleman, J., Whittaker, M., 2004. Alteration of Skin Temperature during Low-Level Laser Irradiation at 830 nm in a Mouse Model. *Photomed. Laser Surg.* 22, 227–231.
Stern, J.M., Kibanov Solomonov, V.V., Sazykina, E., Schwartz, J.A., Gad, S.C., Goodrich, G.P., 2016. Initial evaluation of the safety of nanoshell-directed photothermal therapy in the treatment of prostate disease. *Int. J. Toxicol.* 35, 38–46.
Sung, H., Ferlay, J., Siegel, R.L., Laversanne, M., Soerjomataram, I., Jemal, A., Bray, F., 2021. Global Cancer Statistics 2020: GLOBOCAN Estimates of Incidence and Mortality Worldwide for 36 Cancers in 185 Countries. *CA. Cancer J. Clin.* 71, 209–249.
Sztandera, K., Gorzkiewicz, M., Klajnert-Maculewicz, B., 2019. Gold Nanoparticles in Cancer Treatment. *Mol. Pharm.* 16, 1–23.
Tang, G., Seume, N., Häger, C., Kumstel, S., Abshagen, K., Bleich, A., Vollmar, B., Talbot, S.R., Zhang, X., Zechner, D., 2020. Comparing distress of mouse models for liver damage. *Sci. Rep.* 10, 19814.
Villuendas, H., Vilches, C., Quidant, R., 2022. Influence of Cell Type on the Efficacy of Plasmonic Photothermal Therapy. *ACS Nanosci. Au* 2, 494–502.
Wakayama, C., Inubushi, S., Kunihisa, T., Mizumoto, S., Baba, M., Tanino, H., Cho, I.S., Ooya, T., 2023. Protein corona formation on epigallocatechin gallate-Au nanoparticles suppressed tumor accumulation. *JCIS Open* 9, 100074.
Wang, D., Li, J., Wang, M., Jin, B., Wang, X., Zheng, Y., Liu, B., 2024. Insight into Sonodynamic Activities of Gold Nanoparticles with Different Morphologies. *ChemistrySelect* 9.
Wang, Y., Zhu, K., Wang, J., Yang, L., 2019. Numerical simulation of heat induced flow-mediated dilation of blood vessels. *J. Therm. Biol.* 84, 323–330.
Wong, R.S., 2011. Apoptosis in cancer: from pathogenesis to treatment. *J. Exp. Clin. Cancer Res.* 30, 87.
Worsley, C.M., Veale, R.B., Mayne, E.S., 2022. Inducing apoptosis using chemical treatment and acidic pH, and detecting it using the Annexin V flow cytometric assay. *PLoS One* 17, e0270599.
Xie, X., Shao, X., Gao, F., Jin, H., Zhou, J., Du, L., Zhang, Y., Ouyang, W., Wang, X., Zhao, L., et al., 2011. Effect of hyperthermia on invasion ability and TGF-β1 expression of breast carcinoma MCF-7 cells. *Oncol. Rep.* 25, 1573–1579.
Xie, X., Liao, J., Shao, X., Li, Q., Lin, Y., 2017. The Effect of shape on Cellular Uptake of Gold Nanoparticles in the forms of Stars, Rods, and Triangles. *Sci. Rep.* 7, 3827.

Yun, W.S., Kim, J., Lim, D.-K., Kim, D.-H., Jeon, S.I., Kim, K., 2023. Recent studies and progress in the intratumoral administration of nano-sized drug delivery systems. *Nanomaterials* 13, 2225.
Zhao, X., Qi, T., Kong, C., Hao, M., Wang, Y., Li, J., Liu, B., Gao, Y., Jiang, J., 2018. Photothermal exposure of polydopamine-coated branched Au-Ag nanoparticles induces cell cycle arrest, apoptosis, and autophagy in human bladder cancer cells. *Int. J. Nanomedicine* 13, 6413–6428.
Zhao, L., Zhang, X., Wang, X., Guan, X., Zhang, W., Ma, J., 2021. Recent advances in selective photothermal therapy of tumor. *J. Nanobiotechnology* 19, 335.
Ziegler, U., Groscurth, P., 2004. Morphological Features of Cell Death. *Physiology* 19, 124–128.
Zoio, P., Ventura, S., Leite, M., Oliva, A., 2021. Pigmented Full-Thickness Human Skin Model Based on a Fibroblast-Derived Matrix for Long-Term Studies. *Tissue Eng. Part C Methods* 27, 433–443.